Spatial variations of earthquake occurrence and coseismic deformation in the Upper Rhine Graben, Central Europe

Barth, A.[a], Ritter, J.R.R.[a], Wenzel, F. [a]

[a] Karlsruhe Institute of Technology, Geophysical Institute, Hertzstr. 16, 76187 Karlsruhe, Germany

Corresponding author: Andreas Barth, tel. +49 721 608 44507, email: a.barth@kit.edu

0 Abstract

Seismic activity in the densely populated Upper Rhine Graben (URG) is an aspect in the public, political, and industrial decision making process. The spatial analysis of magnitude-frequency distributions provides valuable information about local seismicity patterns and regional seismic hazard assessment and can be used also as a proxy for coseismic deformation to explore the seismo-tectonic setting of the URG.

We combine five instrumental and one historic earthquake bulletins to obtain for the first time a consistent database for events with local magnitudes $M_L \geq 2.0$ in the whole URG and use it for the determination of magnitude frequencies. The data processing results in a dataset with 274 Poisson distributed instrumentally recorded earthquakes within the URG between 01/1971 and 02/2012 and 34 historic events since the year 1250.

Our analysis reveals significant *b*-value variations along the URG that allow us to differentiate four distinct sections (I-IV) with significant differences in earthquake magnitude distributions: I: Basel region in the Swiss-France-German border region (*b*=0.83), II: region between Mulhouse and Freiburg in the southern URG (*b*=1.42), III: central URG (*b*=0.93), IV: northern URG (*b*=1.06). High *b*-values and thus a relatively low amount of high magnitude events in the Freiburg section are possibly a consequence of strongly segmented, small-scale structures that are not able to accumulate high stresses.

We use the obtained magnitude-frequency distributions and representative source mechanisms for each section to determine coseismic displacement rates. A maximum horizontal displacement rate of

41 μm/a around Basel is found whereas only 8 μm/a are derived for the central and northern URG. A comparison with geodetic and geological constraints implies that the coseismic displacement rates cover less than 10% of the overall displacement rates, suggesting a high amount of aseismic deformation in the URG.

1 Introduction

The Upper Rhine Graben (URG) is a NNE-SSW striking continental rift north of the Alpine mountain chain in the German/French/Swiss border region (Fig. 1). Its total length is about 320 km from Basel/Switzerland in the south to Frankfurt/Germany in the north. The URG evolved due to polyphase tectonic activity since Eocene time (Schumacher, 2002) and it is one of the active seismic regions in Central Europe. The crustal extent of the graben is about 6 km (Meier & Eisbacher, 1991), which mostly took place in Oligocene and Miocene time; present deformation appears to be low (Fuhrmann et al., 2013). Within the rift 22 earthquakes with maximum intensities $I_0 \geq$ VII occurred since 1000 A.D. (Grünthal et al., 2009). The largest known event occurred just south of Basel in 1356 with I_0=IX and M_W 6.9±0.2 (Fäh et al., 2009). The deep geothermal exploitation activity and related induced seismicity within the URG (Evans et al., 2012) cause a demand for local information on recurrence intervals of large tectonic earthquakes, thus providing a measure for the potential of induced seismicity. Furthermore, improved magnitude-frequency relations are an important proxy to estimate the natural seismic hazard in the densely populated URG. Evans et al. (2012) evaluated 41 European injection sites and showed that no induced seismicity occurred at sites with a low seismic hazard potential (less than 10% probability of exceeding 0.08 g within 50 years). On the other hand measures of low magnitude tectonic seismic activity may help to discriminate induced seismicity from natural background seismicity (Dahm et al., 2013). Recent studies on seismic hazard have concentrated on high magnitude earthquakes. The global SHARE-project (e.g. Hiemer et al., 2014) did not take into account magnitudes below M_W 3.7 for calculating magnitude frequencies in Central Europe and the Swiss PEGASOS-project used magnitudes of completeness of

$M_W \geq 2.3$ in the URG (Burkhard & Grünthal, 2009). Because of that and the generally low number of earthquakes in the URG used for the determination of magnitude-frequency relations, national or regional hazard estimations do not permit an analysis of local variability in seismicity. To study spatial changes in the seismic activity we found it necessary to include as many data as possible, i.e. to use small magnitude earthquakes as long as they are known completely above a certain magnitude threshold.

Spatial seismic zonation is an essential basis for the calculation of magnitude-frequency distributions on a regional scale; however recent studies show a different partitioning especially in the N-S subdivision of the URG (Fig. 1, paragraph 2a). New data and a spatial analysis of magnitude-frequency distributions allow us to present an updated systematic zoning of the URG together with an updated determination of recurrence intervals and regional seismic activity.

The oldest documented historic earthquake in the URG is known from 858 A.D. (Leydecker, 2011), with first analogue recordings at the beginning of the 20th century, and a first modern telemetered network installed in 1966 (Bonjer & Fuchs, 1974). Since the 1970's the seismic instrumentation along the URG was constantly improved by state agencies and research institutions. Nowadays, dense seismometer networks with about 40 seismic stations are recording the ground motion of the URG continuously. The seismometers are maintained from different agencies in Germany, France and Switzerland. This instrumental data has decreased the magnitude threshold of earthquake detection and location, providing a valuable dataset for the subdivision of larger into smaller regions with similar seismogenic behaviour. A non-uniform distribution of epicentres in the URG was first recognised by Hiller et al. (1967), and early work including instrumental recordings was summarised in Ahorner & Schneider (1974) and Bonjer et al. (1984). Partly, seismicity can be assigned to known fault systems (Bonjer, 1997a, Behrmann et al., 2003). Based on eight years of instrumental recordings and modern location, Lippert (1979) divided the URG proper into five seismic provinces with varying seismic activity, which was described with the *b*-value of the Gutenberg-Richter distribution (see paragraph 4a): a seismic active northern part (b=0.58), a less seismic active central part (*b*=0.74), the area north of Freiburg (*b*=0.94), the very active southern part (*b*=0.92) and the area around Basel including the Dinkelberg block (*b*=0.88). For the entire URG Lippert (1979) determined *b*=0.74, which is nearly identical to the value of *b*=0.73 for instrumental (1971-1979) and macroseismic (1900-1970) data by Bonjer et al. (1984). Recently Burkhard & Grünthal (2009) assigned a higher *b*-value of 0.858±0.057 to the URG as a large zone and derived a more detailed zone for Basel (*b*=0.894), the Dinkelberg (*b*=0.920), the southern URG (*b*=0.810), and the northern URG (*b*=0.856). A local study using 56 events with magnitudes $M_L \geq 1.3$ in the vicinity of Groß-Gerau resulted in a *b*-value of 0.9 (Homuth et al., 2014). Of course all these *b*-values depend on the regionalisation used and the treatment of the earthquakes catalogues (completeness estimate, handling of fore- and aftershocks, see chapter 3).

The determination of fault plane solutions, their 3-D distribution, and interpretation of the underlying stress field is important for the understanding of recent tectonics and necessary for the calculation of seismic deformation. Generally, mainly strike-slip and normal faulting is observed (Ahorner & Schneider, 1974; Plenefisch & Bonjer, 1997; Ritter et al., 2009; Deichmann & Giardini, 2009; Gaßner et al., 2014). Strike-slip and normal-faulting regimes seem to dominate at different depths: Plenefisch & Bonjer (1997) demonstrate preferred strike-slip in the upper crust and normal faulting in the lower crust of the southern URG, indicating a mechanical decoupling inside the crust.

In the following we combine different earthquake catalogues for the first time to establish a consistent earthquake database for the whole URG. This database reveals spatial changes of earthquake occurrence and permits a revision of existing seismic zonation models. The strain rates in the derived sections of the URG are estimated and discussed in terms of current geodynamic processes. The presented magnitude-frequency distributions are of high relevance for the industry and authorities to estimate the occurrence of local seismicity and might give insights into the recent tectonic development of the URG.

2 Earthquake data and seismic zonations

2a Seismic zonations

Several seismic zonations have been suggested for the URG (Fig. 1, see Leydecker, 2011; Burkhard & Grünthal, 2009; Grünthal & Bosse, 1996; Helm, 1996); they mainly differ in their subdivisions along the rift. Some separate the URG in two, others in three sections. For a southernmost section around the city of Basel, a northern boundary at 47.69°N (~15 km north of Basel) is proposed in Grünthal & Bosse (1996) and at 47.88°N (~10 km south of Freiburg) in Burkard & Grünthal (2009). Helm (1996) used NE-SW striking boundaries as proposed by Grellet et al. (1993) to separate the southern and central part of the URG at about 48.56°N (south of Strasbourg). All authors agree that there is a difference between a northern and a central section of the URG, with a boundary north of Karlsruhe between 49.0°N and 49.3°N. Leydecker (2011) put this boundary at the latitude of Landau (49.19°N) and Helm (1996) used a separating line trending from 49.1°N in the SW to 49.25°N in the NE (Fig. 1). Burkhard & Grünthal (2009) subdivide the central and northern URG at a latitude of about 49.04°N (northern part of Karlsruhe), while Grünthal & Bosse (1996) used a line about 20 km further to the north, south of the city of Speyer (49.23°N). The latter zonation is also used for the German building code DIN 4149 (2005), the official German earthquake zonation, and for the Global Seismic Hazard Assessment Program (GSHAP, Grünthal et al., 1999). In that, most of the URG belongs to earthquake zone 1 (DIN 4149, 2005), i.e. a 10% probability of a maximum intensity I_0=VI-VII earthquake within 50 years. The region south of Freiburg is part of earthquake zone 2 (10% probability of I_0=VII per 50 years), and earthquake zone 3 (10% prob. of I_0=VII-VIII per 50 years) is assigned to Basel and surroundings (Grünthal et al., 1998 and DIN 4149, 2005).

The differences in the cited seismic zonations are mainly based on subjective expertise and are neither well founded nor quantifiable, partly because few earthquakes with only high magnitudes of completeness were available. In this study all available earthquake catalogues are combined, a common magnitude relationship is derived, and variations in the magnitude-frequency relations along the URG are determined to obtain a more reasonable zonation.

2b Earthquake catalogues

To analyse the seismicity of the URG we combine five instrumental catalogues and the historic unified catalogue of earthquakes for central, northern, and northwestern Europe (*CENEC*, Grünthal et al., 2009; Grünthal & Wahlström, 2003). The recent instrumental catalogues are maintained by the Landeserdbebendienst (*LED*) as part of the Landesamt für Geologie, Rohstoffe und Bergbau Baden-Württemberg (*LGRB, state geological service*) in Freiburg, Germany (since 1997), the French collaboration of the Réseau National de Surveillance Sismique (*RéNaSS, state seismological service*) in Strasbourg and the Laboratoire de Détection Géophysique (*LDG*) in Paris (since 1980), the Schweizerischer Erdbebendienst (*SED*, *Swiss Seismological Service*) in Zurich, Switzerland (*ECOS* catalogue, Fäh et al., 2011, here used since 1971) and the Bundesanstalt für Geowissenschaften und Rohstoffe (*BGR*, *Federal Institute for Geosciences and Natural Resources*) in Hannover, Germany (since 1969). In addition, we include the *nrift*-catalogue by K.-P. Bonjer (1997b), which is the precursor of the *LED* bulletin and contains an earthquake catalogue of Southwest Germany since 1971 (Bonjer, 1997a,b). It is also known as the Karlsruhe catalogue. The catalogue of the Hessian Agency for the Environment and Geology (*HLUG*) did contribute only earthquakes below the completeness level of M_L 2.0 (see paragraph 3d).

The basis for our analysis are the yearly bulletins of the *LED*, which have been maintained since 1996 and cover the whole state of Baden-Württemberg and adjacent areas, including the URG. Since 2010 there is a cooperation of the *LED* with the seismic service of the state of Rheinland-Pfalz (Landesamt für Geologie und Bergbau, geological service of Rhineland-Palatinate) called Erdbebendienst Südwest (earthquake service Southwest), which provides earthquake locations in yearly bulletins (1996-2009) and a joint preliminary earthquake list (since 2010). On the German territory our database is complemented with the bulletin of the *BGR* with a few events. As reference we use local magnitudes M_L as given by the *LED* (Stange, 2006, see paragraph 3a).

2c Earthquake distribution

Figure 2 shows the earthquake distribution in the URG scaled by a unified local magnitude M_L and corrected for double events that appear in the different catalogues (see paragraphs 3a-c). In this figure fore- and aftershock as well as induced events are still included to give a complete overview on the seismicity in a wider region surrounding the URG. The instrumental catalogues from 01/1971 until 02/2012 contain 2476 earthquakes within the boundaries of the URG (after Grünthal et al., 1999). The *CENEC* catalogue with historic earthquake contains 145 events within the URG since the year 1080 until 1970 for $M_W \geq 3.5$. The combined catalogue is available as electronic supplementary material. The most striking feature in Fig. 2 is the higher seismicity south of Strasbourg as compared to the northern URG. This observation is true for the instrumental as well as the historical earthquakes. For both groups 75%-76% of the earthquakes are situated south of Strasbourg. Induced seismicity due to deep geothermal operations can be seen clearly around Soultz-sous-Forêst (48.9°N/7.9°E), Landau and neighboring Insheim (49.2°N, 8.1°E) (e.g. Cuenot et al., 2008; see also Barth et al., 2013; Ritter & Groos, 2014). The maximum magnitude event contained in the instrumental catalogue within the URG occurred on 15 July 1980 between Mulhouse and Basel with a magnitude M_L 4.7. The most intense historical earthquake occurred near Basel in 1356 (M_W ~6.9, Fäh et al., 2009).

3 Processing of earthquake data for a consistent earthquake catalogue

To determine magnitude-frequency (or Gutenberg-Richter, GR) distributions, the original earthquake source data have to be processed and filtered to obtain a consistent earthquake database for the whole URG. The following steps will be discussed in this chapter:

- Identification of double listed events
    - Evaluation of the spatial reliability/validity of the catalogues
    - Magnitude conversion
    - Correction for double listed events

- Excluding fore-/aftershocks (declustering) and induced seismicity
- Reducing to URG boundaries
- Determination of magnitude completeness

3a Identification of double listed events

The identification of earthquakes that are double listed in two or more catalogues is an essential task for preparing a consistent earthquake database for several reasons. First, they indicate the reliable spatial coverage of a catalogue into the relevant region of a neighbouring agency and second, they can be used to compare and adapt earthquake magnitudes, originally calculated in different ways by different agencies. In the final database such events can be removed so that each earthquake is included only once in the prioritised database.

3a i) Evaluation of the spatial reliability/validity of the catalogues

It is important to decide to what extent a local earthquake catalogue may be regarded as valid for areas outside its basic coverage, since wrongly localised earthquakes inside the URG may artificially increase the number of events. To estimate the reliability of the *LED* (including its precursor *nrift*) locations in France and vice versa the *RéNaSS* (and *LDG*) locations in Germany, we use both catalogues to create a dataset of earthquakes double listed in both catalogues. Areas, where both agencies determine coincident locations, can be regarded as reliable also for events which are contained in one catalogue. The common procedure to identify double listed events is based on a space-time criterion that assesses the identity of events in different catalogues.

To analyse the space-time similarity between the catalogues given by *LED*, Germany and *RéNaSS*, France, we calculate the spatial distance of epicentres listed in both catalogues. For this first step it is necessary to identify double listed events very accurately, since they will be used as a reference to determine regions of reliable locations in both catalogues and for adapting local magnitudes in both catalogues. For this purpose, we only use events with source time differences of equal or less than 2.0 s. The inclusion of pairs with a higher time difference could lead to biased locations and magnitudes, even though the same event was detected (see paragraph 3a iii). Figure 3 shows the average location difference of double listed events on a grid of 0.2° by 0.2°. To obtain a connected area of good agreement between *LED* and *RéNaSS* locations in the URG, we combine grid cells with average epicentral distances between double listed events of less than 7 km. At the same time only grid cells are chosen that are connected to at least two other cells to get a smooth area of reliable locations of both agencies (double hatched area in Fig. 3). This procedure results in an area along the URG with an east-west extent of up to 120 km at the latitude of Freiburg and around 40 km in the north (Fig. 3). In the north, the area reaches a latitude of 49.35°N on the western side of the river Rhine, near the city of Neustadt a.d.W. The good agreement between the French and German catalogues is mainly due to shared waveform data between the agencies on both sides of the Rhine. Within the above defined area epicentre locations of both agencies are in good agreement. Thus, earthquakes within this area listed only once in either catalogue are included into our final dataset. Other areas of good agreement such as the six grid cells along the French-German border northwest to the URG at 49.2°N and 6.8°E (mining area) are not taken into account.

3a ii) Magnitude conversion

The combination of different earthquake catalogues for the determination of magnitude-frequency distributions requires a consistent magnitude scale for all catalogues. Here, we use the local magnitude M_L, since for most of the data used in this study M_L is provided directly. As a reference we use the *LED* dataset for which $M_{L,LED}$ with appropriate attenuation laws has been derived (Stange, 2006). As a consequence the majority of the magnitude data can be taken directly from *LED* catalogue and do not need any conversion into other magnitude types, which is always a potential source of uncertainty. For the adaption of magnitudes of the other used bulletins we use either the direct comparison of earthquakes apparent in both catalogues (*LED* and an additional one) or direct information about magnitude conversion from the literature. The *nrift catalogue* by Bonjer (1997b) is the direct precursor of the *LED* bulletins. Magnitudes of both catalogues are in good agreement and are not transformed (SED, 2002). The magnitudes of Germany-wide *BGR* catalogue are also not changed because of its conformity to the LED measures. The *ECOS* and *CENEC* catalogues are given as moment magnitudes M_W and need to be converted to $M_{L,LED}$.

For the *RéNaSS* data with $M_{L,RéNaSS}$ a regional relationship to *LED* was estimated using earthquakes apparent in both catalogues. We only use events that occurred within the area of reliable localisations (Fig. 3 and last paragraph) and within the URG to obtain a local relationship valid for our study area. The linear regression of 401 events with magnitudes $1.5 \leq M_{L,LED} \leq 4.7$ between 1980 and 02/2012 is given in Fig. 4. The fitted regression line is

$$M_{L,LED} = 1.14\, M_{L,RéNaSS} - 0.437 \quad . \tag{1}$$

Equation 1 means that, with respect to the *LED* magnitudes, the original $M_{L,RéNaSS}$ values are overestimated below $M_{L,LED}$ 3.1 and underestimated for magnitudes above (Fig. 4).

The *ECOS* earthquake catalogue integrates earthquake sources from historical records (macroseismic magnitudes) since the year 1250 A.D. and instrumental data recorded since 1975 from the Swiss seismic network in Switzerland and bordering countries (Fäh et al., 2011). Beside the southernmost part of the URG around Basel it also covers parts of Southwest Germany up to a latitude of 48.3°N (30 km north of Freiburg). The *ECOS* catalogue by *SED* is generally given in moment magnitudes M_W that, in case of the instrumentally recorded data, originally were converted from local magnitudes M_L. To reconstruct the original local magnitude M_L we use the inverse function of the equation given in the *ECOS* documentation Appendix I (Allmann et al., 2010):

$$M_L = (M_W - 0.985)/0.594, \quad M_W < 2.17$$

$$M_L = \sqrt{M_W/0.085 - 13.4} - 1.49, \quad 2.17 \leq M_L < 3.7$$

$$M_L = M_W + 0.3, \quad M_L \geq 3.7 \quad . \tag{2}$$

As given in the *ECOS* documentation Appendix K (Deichmann, 2009) magnitudes $M_{L,SED}$ since 1996 given by the *SED* show a linear deviation compared to those determined by *LED*, which was empirically determined using 331 magnitudes of earthquakes in Switzerland and Southwest Germany:

$$M_{L,LED} = \left(M_{L,SED} + 0.037\right)/0.964 \quad . \tag{3}$$

By applying equations 2 and 3 on the *SED ECOS* dataset consecutively, the original Swiss magnitudes are adopted to the $M_{L,LED}$ reference scale, which is abbreviated with M_L in the following text.

The moment magnitudes given in the *CENEC* catalogue are converted back into local magnitudes M_L using the relationship given in Grünthal et al. (2009):

$$M_W = 0.0376\, M_L^2 + 0.646\, M_L + 0.53 \quad . \tag{4}$$

In our case the inverse function is used:

$$M_L = \sqrt{M_W/0.0376 + 59.7} - 8.59 \quad . \tag{5}$$

This relation results from the analysis of 221 earthquakes in central Europe. The standard deviation of M_W is about 0.4 and is similar for M_L (Grünthal et al., 2009).

Both equations 2 and 5 agree within the magnitude range M_W 2.7-6.1 with only minor differences below M_L 0.1. Anyhow, the 34 events in the URG (after declustering, see paragraph 3b) used here and taken from the historic catalogue *CENEC* range between M_L 3.8-7.0 (M_W 3.5-6.9), while the *SED ECOS* data include events $M_L \leq 3.0$ (35 events). Due to the non-overlapping magnitude ranges we need no conversion between those different catalogues and equations 2 and 5 can be applied.

3a iii) Correction for double listed events

In order to avoid counting events twice while merging the catalogues, we remove double listed events from the dataset with a slightly weaker space-time criterion than in section 3a i). Here, we assume that two events are the same earthquake, if the source times differ less than 5 s and the epicentres are closer than 15 km. These spatial and temporal criteria are more strict than for the determination of the area with reliable locations from two agencies and the magnitude correlation (sections 3a i) and ii)), since this criterion assures the identification of events with inaccurate location. For building the final dataset the preferred catalogue is the one by *LED*, while the others are prioritised in the following order: *nrift*, *RéNaSS*, *ECOS*, *BGR*, *CENEC*.

3b Removing fore- and aftershocks

We decluster the data by excluding aftershocks, earthquake series (except for the strongest event, which is considered as the main event), and seismicity related to man-made activity. This step leads to a dataset of timely independent, i.e. Poisson distributed (see below), earthquakes, which is commonly used for seismic hazard assessment (e.g. Hiemer et al., 2014). For identifying fore- and aftershocks we use the equations given by Burkhard & Grünthal (2009), which are based upon empirical formulas for central European earthquakes and have been validated during the PEGASOS-project. Accordingly, for each mainshock a magnitude dependent time and space window for fore- and aftershocks can be calculated, respectively. The foreshock time window is given by

$$dT_f(M_W) = \exp\left(-4.77 + \sqrt{0.62 + 17.32\,M_W}\right) \quad , \qquad (6)$$

while aftershocks are found during a longer period:

$$dT_a(M_W) = \exp\left(-3.95 + \sqrt{0.62 + 17.32\,M_W}\right) \quad . \qquad (7)$$

The radius within fore- and aftershocks occur is

$$dR(M_W) = \exp\left(1.77 + \sqrt{0.037 + 1.02\,M_W}\right) \quad . \qquad (8)$$

For applying equations 6 to 8, we transfer the homogenised local magnitudes M_L to moment magnitudes M_W using eq. 4. Within the URG the declustering removes fore- and aftershocks of 247 earthquake series from the dataset. In addition 96 events $M_L \geq 2.0$ are assigned to induced seismicity by geothermal injections during the recent years. Finally, this results in a reduction from 2476 to 1135 events between 01/1971 and 02/2012. The final dataset of instrumentally recorded earthquakes consists of 513 events from the *nrift*-catalogue, 320 by *LED*, 232 by *RéNaSS*, 35 by *ECOS*, 32 by *BGR*, 3 by *HLUG* and 107 historic events by *CENEC* (see electronic supplement).

3c Reducing to URG boundaries

For reducing the dataset to the URG proper, we use the boundaries of the German Earthquake Hazard Map DIN 4149, which is the official zonation and mostly coinciding with the graben shoulders (Grünthal & Bosse, 1996; after GSHAP, Grünthal et al., 2009, see Fig. 1). In the east and west the boundaries run along the shoulders of the URG. They reach Frankfurt in the north and terminate approx. 15 km south of Basel. The region southwest of Mulhouse (Dannemarie Basin) is part of the transition zone to the Bresse Graben and therefore not regarded as a part of the URG (Rotstein et al., 2005b). The study region has a width of about 35 km around Basel and about 45 km further north; and it is 320 km long in NNE-SSW direction (Fig. 1, white solid line).

3d Determination of magnitude completeness

Presently the URG is covered by about 40 seismic stations from different agencies and research institutions to record and locate earthquakes continuously. Since the 1970s the coverage has been increasing steadily and therefore we introduce a time variable magnitude of completeness M_C to calculate the local *b*-value. To determine M_C for the time interval 1971-2012 we plot the cumulative number of earthquakes for the magnitude range $1.8 \leq M_L \leq 2.2$ over time for the whole URG (Fig. 5). Roughly linear segments reveal periods with a constant observation rate, increasing gradients indicate increasing observation rates (Burkhard & Grünthal, 2009). The higher the chosen threshold M_C, the less continuous the point curve becomes. The black circles corresponds to earthquakes with $1.95 \leq M_L \leq 2.05$ and show several steps, due to the limited number of earthquakes (70 since 1971). However, the observed gradient changes systematically only between 1980 and 1982. To obtain a stable M_C for the low number of data, we crosscheck the magnitude completeness of the year 1982 by fitting different magnitude ranges by a Gutenberg-Richter distribution (chapter 4) as proposed by Mignan & Wössner (2012). Figure 6 demonstrates the significant improvement of the fit (decrease of chi-squared) for magnitudes $M_L \geq 2.0$ (containing 265 events). Thus, the magnitude of completeness for 1982 was assessed to M_L 2.0. The constant chi-squared level for higher magnitude ranges indicates the stability of the Gutenberg-Richter distribution. The further, slight decrease of chi-squared for higher magnitudes is due to the low data number of about 50 events and less.

For the beginning of the instrumental earthquake localisation in 1971 and for historical times we adapt the values given in Burkhard & Grünthal (2009) for Southwest Germany (Table 1).

Table 1: Magnitude of completeness in units of M_L and assigned time period.

Time since	M_C
1982	2.0
1971	3.0
1865	3.8
1650	5.8
1250	6.8

The final dataset consists of 274 instrumentally localised earthquakes and 34 historic events. This increase of the data number compared to previous studies allows us to perform a stable spatial analysis of *b*-value changes along the URG.

The processing described in the previous paragraphs results in a Poisson distributed (time independent) dataset. To demonstrate this, we determine the number of earthquakes with $M_L \geq 2.0$ in each 2-months period since 1982 and count how many of these periods contain a given number of earthquakes. This distribution in time can now be compared to the theoretical Poisson distribution for the overall number of events. Fig. 7 shows the comparison between real data and a Poisson distribution for the original earthquake list containing fore- and aftershocks (Fig. 7a) and the declustered final dataset (Fig. 7b). The chi-squared test for the clustered dataset with respect to a Poisson distribution results in a value as large as 10^{22}, indicating no agreement. However, after declustering a value of 2.2 is achieved, which corresponds to a 90% significance level that the data is Poisson distributed. The successful data processing allows a spatial analysis of the magnitude distribution for the URG and thus can be used for regional seismic hazard assessment.

4 Results

4a Gutenberg -Richter distribution

To analyse the magnitude frequency or Gutenberg-Richter (GR) distribution we apply the maximum likelihood estimation after Aki (1965) and Utsu (1965):

$$b = \left(\bar{M} - M_C\right)^{-1} \cdot \log e \quad , \qquad (9)$$

with the mean magnitude $\bar{M}$ and the magnitude of completeness M_C. Equation 9 is derived from the classical GR relation

$$\log N = a - b \cdot M \quad , \qquad (10)$$

under the assumption that the datasets represents a population obeying the Poisson distribution (time independent events as shown above). N denotes the rate of events larger than magnitude M (cumulative exceedance frequency).

To apply this method to time periods with M_C (Tab. 1), we use the formulation of Weichert (1980). Because of the low data number, we use cumulative statistics for the event numbers (analysis of magnitudes levels above a certain threshold), that are less affected by large steps in the distribution function than incremental representations (magnitude levels between certain boundaries).

The GR distribution of the whole URG separated for instrumental and historic data is shown in

Fig. 8a. The *b*-value calculation following eq. 9 varies strongly and results in b_{instr}=1.05 and b_{hist}=0.59, respectively.

4b Historic magnitudes

Historic magnitudes have a higher uncertainty than recent instrumental measures, since estimates are based on historic reports of damage and perceptibility. The standard deviation of the magnitude values in the historic earthquake catalogue CENEC, used in this study, is 0.4 magnitude units (Grünthal et al., 2009). As shown in Fig. 8a the straight forward combination of instrumental (beginning in 1970) and historic (1250-1970) magnitude information does not fit to a common GR relation for the URG. In order to achieve a consistent GR distribution between instrumental and historic magnitude values, we analyse the magnitude shift between both catalogues using a chi-squared test (Fig. 8b). The best fit is obtained, if historic magnitude values $M_{L,hist}$ are shifted with respect to instrumental ones by -0.4 magnitude units, which is equal to the standard deviation of $M_{L,hist}$. For reasons of comparability with instrumental earthquake source data, we adapt the overestimated historic magnitudes $M_{L,hist}$ by a correction term $\Delta M_{L,hist}$ and leave instrumentally determined magnitudes unchanged. A special treatment is applied to the largest earthquake in Basel, 1356. Since Fäh et al. (2009) determined a standard deviation of 0.2 magnitude units, the event magnitude is only decreased by $\Delta M_{L,hist}$=-0.2. A recent study of two historic events west of Karlsruhe near Kandel in 1880 and 1903 revealed an overestimation of 0.5 and 1.1 magnitude units, respectively (Barth, 2011), which are due to local generalisations of singular intensity observations. This result might be a hint for a systematic overestimation of historic magnitudes and needs further investigation.

4c Local variation of the b-value

With the adaption of $M_{L,hist}$ for the historic data the final GR relation for 308 earthquakes in the whole URG is

$$\log N = 2.874 - 0.993 \cdot M_L \quad , \tag{11}$$

with a standard deviation *σ(b)*=0.037 (formula by Weichert, 1980). This value is somewhat higher than *b*=0.858±0.057 of Burkhard & Grünthal (2009) who used M_C=2.3 and clearly higher than the value of 0.73 of Bonjer et al. (1984) using a much sparser dataset. Thus, 7.7 earthquakes with $M_L \geq 2.0$ occur on average per year. The average return period *T* for earthquakes with $M_L \geq 3.0$ and with $M_L \geq 4.0$ is 1.3 years and 12.5 years, respectively.

To analyse the spatial variation of the *b*-value along the URG, we use a spatial sliding window that covers the whole east-west width of the URG and that has a north-south extent such that at least 50 instrumentally localised earthquakes plus historic events are contained within it. Starting at the southern rim of the URG the southern boundary of the spatial window is shifted northwards by 0.01 degree in latitude stepwise to obtain a continuous record of the GR parameters. This analysis gains 172 overlapping subregions of the URG with different north-south extent depending on earthquake density. The continuous maximum-likelihood *b*-value estimation after Weichert (1980) within the spatial windows reveals local variations of the *b*-value. In the southern URG the *b*-value increases from 0.74±0.06 around Basel to a maximum value of 1.49±0.16 around Freiburg (Fig. 9b). High *b*-values indicate a high ratio of lower to higher magnitude earthquakes. Thus, the average event rate $v(M_L \geq 2.0)$ has a maximum around Freiburg of 1.6 events per year per 1000 km² (corresponding to a 23 km north-south extent across the URG, Fig. 9c), while magnitudes $M_L \geq 4.0$ have a minimum average value of v=0.016 a^{-1} 1000 km^{-2} (Fig. 9d). The average return period *T* within 1000 km² is given as

$$T = \nu^{-1} \quad , \tag{12}$$

and thus $T(M_L \geq 4.0)$=63 a within 1000 km². The central and northern parts of the URG are characterised by less pronounced *b*-value changes between 0.87±0.08 (Strasbourg to Karlsruhe) and 1.06±0.10 (north of Karlsruhe), with varying average event rates of $v(M_L \geq 2.0)$=2-7 a^{-1} 1000 km^{-2}

and average spatial return periods of $T(M_L \geq 4.0)$=11-50 a·1000 km². Extending the GR relation to magnitudes below M_C reveals high average event rates of as many as $v(M_L \geq 1.0)=50\ a^{-1}\ 1000\ km^{-2}$ around Freiburg (Fig. 9b), corresponding to the higher amount of (incomplete) observed events in that region (Fig. 9a).

In addition, Figure 9b shows the influence of strong historic earthquakes and the declustering process by the dotted and dashed lines, respectively. Using a constant magnitude of completeness M_C for the whole URG the *b*-value is a direct function of the mean magnitude $\bar{M}$ (see eq. 9). Thus, neither single historic earthquakes, nor the number of fore- and aftershocks does change the significant *b*-value variation in the southern URG. However, an increase of the *b*-value due to strong historic events can be seen in the central and northern part of the study region. The significant *b*-value change for the declustered dataset north of 49.6°N to values as low as *b*=0.86 is due to the Groß-Gerau earthquake swarm 1869-71 that produced eleven events $M_W \geq 3.5$ (Grünthal et al., 2009).

The derived variations in *b*-value along the URG allow a quantitative separation in four sections (I-IV), according to the four extrema in Fig. 9b. For separating sections the spatial extent of the four sections around the *b*-value maxima and minima are evaluated. The first minimum around Basel (section I) is allocated to an area from 47.41°N to 47.69°N, while the maximum value near Freiburg (section II) is located between 47.82°N and 48.01°N. The centre between the two extrema is at 47.76°N (near Mulhouse, Fig. 9b), separating the sections I and II around the highest *b*-value gradient. To derive the northern border of section II around Freiburg, the local minimum in *b*-value variation of the spatial window between 48.10°N and 48.45°N is used. The centre between the two sections II and III is located about 7 km north of Freiburg at 48.06°N, which marks the transition from high to intermediate *b*-values. The third separation between the central (section III) and the northern (section IV) part of the URG is less distinct, since the spatial windows around the minimum of *b*=0.87 (48.31°N-49.19°N) and the maximum of *b*=1.06 (49.09°N-50.14°N) overlap. Thus, we define a transition zone between the two sections ranging from 49.09°N to 49.19°N (i.e. from 5 km north of Karlsruhe to Landau). Table 2 summarises this separation and gives *b*-value calculations for each section. For simplicity *b*-values for sections C-URG and N-URG are calculated for an average common boundary at 49.14°N.

Table 2: Magnitude-frequency distributions for the sections I-IV of the URG.

Region (Section)	**N-S dimensions**	**Number of events**	***b*-value**	***a*-value**	**Average event rate $M_L \geq 2.0$**	**Average return period $M_L \geq 4.0$**
Basel (I)	47.39°N - 47.76°N	81	0.83 ±0.06	1.92	1.82 a^{-1} (1.27 a^{-1} 1000 km^{-2})	25.1 a (36.1 a·1000 km²)
Freiburg (II)	47.76°N - 48.06°N	75	1.42 ±0.12	3.14	2.00 a^{-1} (1.36 a^{-1} 1000 km^{-2})	347 a (507 a·1000 km²)
Central URG (III)	48.06°N - 49.14°N	100	0.93 ±0.06	2.24	2.40 a^{-1} (0.46 a^{-1} 1000 km^{-2})	30.2 a (156 a·1000 km²)
Northern URG (IV)	49.14°N - 50.21°N	52	1.06 ±0.10	2.27	1.35 a^{-1} (0.23 a^{-1} 1000 km^{-2})	102 a (596 a·1000 km²)
Total URG (I-IV)	*47.39°N - 50.21°N*	*308*	*0.99 ±0.04*	*2.87*	*7.72 a^{-1} (0.56 a^{-1} 1000 km^{-2})*	*12.5 a (174 a·1000 km²)*

4d Seismic displacement rates

The recovered distribution of the seismicity in the URG allows new insights into the current tectonic activity of the region. To calculate seismic deformation and displacement rates, we combine GR relations and representative source mechanisms for each region (Schmedes et al., 2005). Magnitude frequencies represent the general distribution of seismicity up to time scales of a seismic cycle and thus are more appropriate for such calculations than instrumentally recorded seismicity alone. To cover the deformation released by all earthquakes, we use a GR relation that includes fore- and aftershocks (compare Fig. 9b). Since earthquake source mechanisms seem to change from strike slip to normal faulting with depth in the URG (Plenefisch & Bonjer, 1997), we reduce our dataset to upper crustal seismicity. Thus, only events with hypocentres above 15 km depth are considered, because the depth range of 0-15 km corresponds to the upper crust in the URG (Prodehl et al., 1976, Wenzel & Brun, 1991; Mayer et al., 1997). The resulting *b*-values using all events in the upper crust of the southern URG are similar to those of the declustered dataset for the entire crust (Tab. 2) and lie within one standard deviation of the latter. For section I (Basel) the *b*-value is enlarged by 0.03 (b=0.87), for section II (Freiburg) the b-value remains unchanged (b=1.42), and for section III (C-URG) it differs by 0.06 (b=1.00) for the upper crust events relative to the entire crust. Only for section IV (N-URG) a significant decrease by 0.17 to b=0.90 is apparent that is caused by ten additional historic events $M_L \geq 3.8$ during the earthquake series of Groß-Gerau 1869-1871.

Kostrov (1974) showed that the average seismic strain rate tensor $\dot{\boldsymbol{\epsilon}}$ can be calculated by summing all moment tensors $\boldsymbol{M}$ that occurred inside a seismogenic volume V within a time period t:

$$\dot{\epsilon}_{ij} = \frac{\sum M_{ij}}{2\mu V t} \quad , \tag{13}$$

with the average shear modulus μ of the rock material. After Jackson & McKenzie (1988) the eigenvalue λ_T, corresponding to the tension axis of the summed moment tensors, can be used to calculate the strain rate $\dot{\epsilon}_T$ parallel to the direction of extension:

$$\dot{\epsilon}_T = \frac{\lambda_T}{2\mu V t} \quad . \tag{14}$$

Thus the displacement rate v_T, which is parallel to the orientation of the tensional principal strain axis, can then be determined by

$$v_T = \dot{\epsilon}_T \cdot w = \frac{\lambda_T}{2\mu d L t} \tag{15}$$

for the volume V. In our case V corresponds to the product of the graben width w of the URG, the length L of the URG sections I-IV and the seismogenic depth d=15 km. Fig. 10 shows the depth distribution of the earthquake hypocentres in our dataset. While lower crustal seismicity (d > 15 km) is apparent in the two southern sections around Freiburg and Basel (Bonjer, 1997a) as well as in the northern URG (Ritter et al., 2009; Homuth et al., 2014), below the central URG there are only intermediate depth earthquakes with hypocentres down to d ≤ 15 km.

We use the GR distributions for the URG (Table 2) to calculate an average cumulative seismic moment rate $\dot{m}_0^c$ for each section I-IV, that can be assigned to representative source mechanisms to determine the average strain rate tensor (eq. 13). Since events with large magnitudes dominate the calculation of the cumulative seismic moment rate, we use a truncated GR relation (Page, 1968; Burkhard & Grünthal, 2009), which is commonly used in seismic hazard assessment:

$$N(M) = N(M_0)\cdot\frac{\exp(-\beta(M-M_0))-\exp(-\beta(M_{max}-M_0))}{1-\exp(-\beta(M_{max}-M_0))} \quad , \tag{16}$$

with $\beta = b\cdot\ln(10)$.

Equation 16 must be transferred to an incremental form to assign seismic moments to each magnitude step in the GR distribution:

$$\begin{aligned} N'(M) &= N'(M-\Delta M \le M_W < M) \\ &= N(M_0)\cdot\frac{\exp(-\beta(M-\Delta M-M_0))-\exp(-\beta(M-M_0))}{1-\exp(-\beta(M_{max}-M_0))} \\ &= N(M_0)\cdot\frac{\exp(-\beta(M-M_0))}{1-\exp(-\beta(M_{max}-M_0))}\cdot(\exp(\beta\Delta M)-1) \end{aligned} \quad . \tag{17}$$

The obtained incremental rates *N'* are multiplied with the related seismic moment

$$m_0(M) = 10^{1.5(M+6.06)} \tag{18}$$

to achieve the cumulative seismic moment rate for each section of the URG :

$$\dot{m}_0^c = \sum_{M=M_0}^{M_{max}} N'(M)\cdot m_0(M) \quad . \tag{19}$$

To determine the average displacement rate in the sections, the geometry of representative faults must be included. The URG appears to be dominated by a general transtensional stress regime (Cardozo & Behrmann, 2006). In all sections I-IV mainly strike-slip source mechanisms occur and only a minor amount of normal faulting earthquakes are known in the upper crust (Peters, 2007; Plenefisch & Bonjer, 1997; Bonjer, 1997a; Delacou et al., 2004; Barth et al., 2009, Homuth et al., 2014). We use two idealised representative focal mechanisms for each section of the URG that are weighted according to their occurrence frequency and that vary concerning their dip angles. In the northern URG Bonjer et al. (1984) calculated normal faulting mechanisms with strike orientations around 150°E. Additionally, Homuth et al. (2014) determined a dominant orientation of focal mechanism tension axes of 45-60°E, corresponding to a strike of 135-150°E for extensional structures. We assign 30% of the seismicity section IV to an average normal faulting mechanism with a 60° dipping fault plane that strikes 140°E, while 70% are represented by strike-slip mechanisms, with fault planes striking 10°E (Peters, 2007; Bonjer et al., 1984; Ritter et al., 2009; Cardozo & Behrmann, 2006).

For sections I-III between Basel and Karlsruhe we adopt the results of Plenefisch & Bonjer (1997), who determined around 70% strike-slip mechanisms, striking around 10°E and 30% normal faulting mechanisms (strike 120°E, dip 60°). Similar results were given by Peters (2007), Bonjer (1997a), and Delacou et al. (2004).

For our four sections of the URG (Table 2) we assign the cumulative seismic moment rates to the representative focal mechanisms by eq. 19. As mentioned above the calculation of the cumulative seismic moment is governed by large magnitudes and thus the assumed maximum magnitude. To preserve the comparability of the strain rate calculations we use a common maximum magnitude M_{max} of M_W 6.5 for the whole URG (Burkhard & Grünthal, 2009). Combined with an average shear modulus of μ=3 10^{10} Pa and the geographical properties of the URG sections we calculate the strain rate tensors and displacement rates (eq. 15) as shown in Table 3.

The highest displacement rates are found in section I (Basel area) with an average horizontal displacement rate $v_{t,hor}$=41.2±2.8 μm/a, due to the low *b*-value and accordingly high average rates of large earthquakes. This maximum extensional strain has an orientation of 51°E with an uncertainty of 20°, which corresponds to a conservative estimation of the accuracy of focal mechanism determination due to varying fault orientation (Barth et al., 2008). The vertical displacement rate is ten times less because of the predominant strike slip mechanisms. A much lower horizontal displacement rate results for section II (Freiburg area) with $v_{t,hor}$=1.20±0.08 μm/a. The sections III and IV (C-URG and N-URG) are characterised by intermediate rates with $v_{t,hor}$=8.15+0.56 μm/a and

$v_{t,hor}$=8.36+0.84 µm/a, respectively. Vertical displacement rates describe the subsidence within the four sections. Due to the regional tectonics, which are accounted for by the representative focal mechanisms, horizontal displacement rates are about one order higher than vertical ones, which vary between 0.1 µm/a and 4.8 µm/a (Table 3). This effect depends on the dip of the normal faulting rupture planes. For steeper planes the vertical component of the tensional strain increases, while it decreases for shallower planes. To show this dependency and to estimate the variability of our results given above, we calculate the seismic displacement rates for sets of normal faulting mechanisms with 40° and 80° dipping fault planes, which is a ±20° variation of the average value (see above). Figure 11 and Table 3 show the variation of seismic displacement rates for 40°, 60°, and 80° dipping fault planes for each section of the URG. Accordingly, the vertical rates may vary between 5% and 25% of the horizontal ones. Absolute values of seismic displacement however, depend strongly on the choice of the maximum magnitude M_{max}. In the case of section I around Basel a change of 0.2 magnitude units would result in a 36% increase, 0.5 units in a 123% increase of the cumulative seismic moment and thus the seismic displacement rate.

Table 3: Seismic displacement rates for the sections of the URG based on the representative focal mechanisms and GR relations. Variations result of a 20° dip variation (see text).

Region (Section)	**N-S dimensions**	**E-W width in km**	**N-S length in km**	**Cum. seismic moment rate in Nm a^{-1}**	**Vertical subsidence rate in µm a^{-1}**	**Horizontal displacement rate in µm a^{-1} (orientation)**	**Horizontal strain rate in nm m^{-1} a^{-1}**
Basel (I)	47.39°N - 47.76°N	35	41	1.63e15	4.81±4.15	41.19±2.8 (51°E)	1.18
Freiburg (II)	47.76°N - 48.06°N	44	33	3.84e13	0.14±0.12	1.20±0.08 (51°E)	0.03
Central URG (III)	48.06°N - 49.14°N	45	120	9.47e14	0.95±0.82	8.15±0.56 (51°E)	0.18
Northern URG (IV)	49.14°N - 50.21°N	47	119	9.24e14	1.01±0.87	8.36±0.63 (54°E)	0.18

5 Discussion

5a Distribution of seismicity

The URG seismicity in Fig. 2 is characterised by a clear decrease in number of events from the southern URG towards the northern URG, as reported previously (Bonjer & Fuchs, 1974; Bonjer et al., 1984). We found the highest cumulative seismic moment rate (1.63 10^{15} Nm a^{-1}, see Table 3) in section I around Basel. This zone is situated closest to the Alps and consequently influenced by the Alpine tectonics in two ways: the steep Alpine topography towards south adds a vertical stress component and the closer position to the Alpine collision zone relative to the northern sectors of the URG may result in higher horizontal stresses. A spatial stress variation was observed with near-surface stress measurements by Greiner & Illies (1977) who describe a decreasing gradient of horizontal tectonic stress from the Central Alps to the northern foreland. Likewise, Becker & Paladini (1990) mapped decreasing horizontal near-surface stress magnitudes from the southern URG with 2-4 MPa to the northern URG with 0-2 MPa, which further decreases to negative values (-2 MPa, extension) towards the Rhenish Massif. This finding was supported by Müller et al. (1997) who speculate about “an increase of shear stress by increased collisional stress close to the Alps”. Reinecker et al. (2010) find indications that the horizontal stress in the Alpine foreland is controlled by the gravitational potential energy due to the Alpine topography. Therefore we attribute the relatively increased seismicity rate in the southern URG to the influence of tectonic stresses related to convergence in the Alpine collision zone and to topography. This interpretation is consistent with observed geodetic strain rates, which are larger in and around the Alps than in the foreland (Tesauro et al., 2006; Kreemer et al., 2014).

5b Spatial b-value and magnitude frequency variation

The *b*-value analysis of 308 instrumentally recorded and historic earthquakes illustrates a variation between 0.83 and 1.42 along the URG (Fig. 9b) with a generally decreasing frequency of earthquake occurrence for $M_L < 2.0$ (Table 2, Fig. 9c) from south to north. Previous results for the *b*-

value in the seismically high active southernmost URG of 0.89-0.92 (Burkhard & Grünthal, 2009; Lippert, 1979) are similar to our calculations for section I (b=0.83±0.06). The clearly greater *b*-value around the Freiburg region, reaching a maximum value of 1.42, is well resolved by our sliding moving window technique (see paragraph 4c) and exceeds the previously known *b*-values. However, previous studies found *b*-values of 0.58-0.856 for the central and northern URG (Lippert, 1979; Bonjer et al., 1984; Burkhard & Grünthal, 2009) that are lower than our results of 0.93 and 1.06, respectively. Beside the influence of the fitting techniques, the main reason for that difference is the enlarged dataset in our study, including magnitudes $M_L \geq 2.0$, which allows a more precise *b*-value determination compared to previous work on intermediate level seismicity in this region.

Around Freiburg (section II) the increased *b*-value reflects the less frequent occurrence of earthquakes with magnitudes $M_L \geq 3.0$, while weaker earthquakes ($1.0 \leq M_L \leq 2.0$) are more abundant compared to the sections I and III towards south and north. Although events with magnitudes $M_L < 2.0$ are not included into the *b*-value analysis (since this range is not observed completely), the observed accumulation of low magnitude events around Freiburg (compare Fig. 9c) and the general seismicity pattern (Fig. 2) support this result. The increased *b*-value in section II and the associated increase in weak seismicity may reflect preferred small-scale ruptures of about 10-100 m length (magnitude-length relation after Bohnhoff et al., 2010). Edel et al. (2006) also described an increased seismicity rate in the region and speculated about a ramp-like wedge. Alternatively, such an accumulation of weak seismicity might be a consequence of the interplay between the tectonic background stress field and relatively small-scale block structures in the upper crust that could prevent regional stresses to build up to levels at which strong earthquakes would be produced. In section II tilted fault blocks above a major west-dipping master fault are commonly cut by WNW-striking transfer faults, inducing an intense segmentation of NNE-trending fault blocks (Eisbacher, pers.-comm.; Fielitz et al., 2014).

This is supported by similarly dissected tilted and faulted blocks on the westside of the graben in section II near the Western main boundary fault (Rotstein & Schaming, 2008). In section I south of

Mulhouse stronger events occur in a region of rather large structures south of Mulhouse (i.e. the Dannemarie Basin and the Mulhouse High, Fig. 12, compare Rotstein et al., 2005a,b), while northwards in section II there is a decreased number of large earthquakes. Detailed fault structures in the central graben segment between the Sierentz fault and the Rhine river are not well known (Rotstein et al., 2005a).

On the eastern side of the graben around Freiburg the URG is segmented into blocks on a scale of a few kilometres; some of the bounding faults may be seismically active, while known seismicity is distributed between the boundary faults and faults inside the URG (Bonjer, 1997a; Behrmann et al., 2003). However, a clear correlation of single earthquakes with displacements on specific faults is not yet possible, since the uncertainties of the event locations and of the positions of inclined fault planes at depth are still too large. One peculiarity in this part of the southern URG is an accumulation of seismicity within the inner graben (Bonjer, 1997a; Edel et al., 2006), which may correspond to an activation of the Rhine River fault (or inner boundary fault according to Bonjer, 1997a) or reflect ongoing displacements along a major west-dipping fault separating a deep basin in the west from a shallow marginal block in the east (Eisbacher, pers. comm.). However, to determine seismo-tectonic details, more local seismicity recordings are required to achieve a much better resolution of hypocentre parameters. Thus, fore- and aftershock distributions as well as new earthquake focal mechanisms could be determined to locate the most active fault planes.

5c Coseismic and aseismic deformation

We calculated coseismic displacement rates in the URG which amount to 0.1-4.8 µm/a subsidence and 1-41.2 µm/a horizontal displacement (Table 3). Even within the error bounds, which mainly dependent on the assumed maximum magnitude, the coseismic horizontal displacement rates are restricted to less than 100 µm/a. There is a clear variation along the URG with the highest coseismic displacement rates in the south (section I) while it is very small (< 10 µm/a) towards north (sections II-IV). Our coseismic displacement rates are quite low compared to values derived from geologic and geodetic indicators, which support the picture of an actively subsiding graben. Peters (2007) calculated 60-125 µm/a relative vertical displacement from uplift of fluvial terraces during the last 800 ka for distinct regions in the northwestern URG, which might be an indicator for graben subsidence. In the Heidelberg basin along the eastern edge of the northern URG, up to 990 m of sedimentary rock could have accumulated since about 2.5 Ma (Buness et al., 2008), corresponding to a local subsidence rate of about 400 µm/a. Similar results were obtained by geodetic levelling campaigns covering some tens of years that identified about 200-300 µm/a subsidence for the central URG and 400-700 µm/a at the eastern and western margins (Prinz & Schwarz, 1968; Bartz, 1974). Nivière et al. (2008) estimated maximum slip rates during Quaternary times of 40-180 µm/a for individual faults in the Freiburg region. A recent study by Fuhrmann et al. (2014) combined data from various levelling surveys and determined tectonic vertical subsidence rates in parts of the central and southern URG of about −200 µm/a to −500 µm/a (±200 µm/a) that possibly include significant compaction of the sedimentary graben fill. Some of these rates are about two orders of magnitude higher than the coseismic vertical displacement rates shown in Table 3.

Horizontal displacement rates are more difficult to obtain, since data from the widely used Global Navigation Satellite Systems (GNSS) have become available only in recent years. Fuhrmann et al. (2013) determined horizontal displacement rates that are mainly less than 500 µm/a in Southwest Germany. They combined six to eight years long GNSS time series from different agencies and obtained a formal error of less than 100 µm/a, thus confirming previous studies, which suggest that horizontal extension rates in the URG do not exceed 1000 µm/a (Rosza et al., 2005; Tesauro et al., 2006).

The strong variability on geodetically determined vertical displacement rates and sparse information on horizontal rates in the URG do not allow detailed comparisons with the coseismic displacement rates estimated in this study. To explain a conservatively assumed overall displacement rate of 500 µm/a (see above) only by coseismic deformation, it would require for example a maximum magnitude of M_w 8.0 in section I or M_w 9.3 in section III. However, such magnitudes are far beyond the realistic value of M_W 6.5 assumed in this study. Therefore, our estimates suggest a high degree of aseismic deformation in the slowly opening URG with coseismic displacement rates below 50 μm/a covering less than 10% of the overall displacement rates (compare Table 3). The low seismic displacement rates in section II around Freiburg might be a hint to a mainly aseismic deformation along strongly partitioned faults, which are oriented both parallel and transverse to the main boundary faults of the URG (Fig. 12).

6 Conclusion & Summary

The current availability of instrumentally localised seismicity combined with historic earthquake catalogues allows a determination of the spatial variation of occurrence rates in the URG even for small earthquakes. To achieve this objective, we compiled a combined dataset from one historic and five instrumental earthquake catalogues with local magnitudes as low as M_L 2.0. Overall, we cover a broad range of magnitudes (M_L 2.0-7.0) for the determination of magnitude frequencies of perceptible seismicity on a local scale. The analysis of the new dataset results in a spatial variation of the *b*-value, which is used to derive four new seismo-tectonic sections within the URG, the return periods for earthquakes and the average coseismic displacement rates in the upper crust.

For consistency we adapted the magnitudes of the combined dataset to the M_L reference scale provided by the Landeserdbebendienst Baden-Württemberg (Stange, 2006). The dataset was cleaned from double listed events, and fore- and aftershocks were removed by a declustering process that resulted in a Poisson distributed data catalogue with 274 instrumentally localised and 34 historic earthquakes. The evaluation of the spatial *b*-value variation reveals four seismo-tectonic sections. Section I covers the area around Basel with a *b*-value of 0.83±0.06. Further north from Mulhouse to around 7 km north of Freiburg section II is located with b=1.42±0.12. Two larger sections of approx. 120 km N-S extent include the central and northern URG (sections III and IV). They are separated by a transition zone between Karlsruhe and Landau and are characterised by values of *b*=0.93±0.06 and *b*=1.06±0.10, respectively. For the whole URG we obtained a *b*-value of 0.99±0.04.

The new dataset and the derived *b*-values (Table 2) allow us to estimate average occurrence rates for earthquakes with different M_L in the four sections. E.g. a $M_L \geq 2.0$ earthquake, as a proxy for a felt shallow earthquake in the URG, is five times more frequent in the southern URG (sections I and II: 1.27 events per year and per 1000 km^2 and 1.36 events a^{-1} 1000 km^{-2}, respectively) than in the northern URG (section IV: 0.23 a^{-1} 1000 km^{-2}). In the central URG between Freiburg and Karlsruhe (section III: 0.46 events a^{-1} 1000 km^{-2}) the activity of perceptible events is twice the activity in the northern URG (section IV). The average rates of larger earthquakes ($M_L \geq 3.0$, Fig. 9d) indicate that in the southernmost URG (section I) ten times more events occur than in the northern URG (section IV). Section II around Freiburg is characterised by a high *b*-value and thus a low occurrence rate of earthquakes with $M_L \geq 3.0$ and especially for $M_L \geq 4.0$. This magnitude-frequency distribution may be due to strongly partitioned subsidence of relatively small crustal blocks compared to the other sectors (Fig. 12). Therefore, tectonic stress in section II might be distributed on smaller fault segments that are not capable of accumulating stress large enough to be released by larger earthquakes. This means that events with $M_L \geq 4.0$ occur rarely in section II, because their average return period of about 350 a is clearly much longer compared to the adjoining sections (I: 25 a, III: 30 a). The shortest return period in section I around Basel is explained with increased stress due to the proximity to the compressive stress field of the Alps.

We calculated the average upper crustal coseismic deformation rate in the four seismo-tectonic sections of the URG using the new magnitude-frequency distributions in Table 2 and representative normal and strike-slip focal mechanisms. Vertical subsidence rates range between 0.1 µm/a and 4.8 µm/a, while horizontal displacement rates are about ten times higher reaching 1 µm/a to 41.2 µm/a. This difference is a result of representative focal mechanisms we used, reflecting the generally transtensional tectonics in the URG with a higher percentage of horizontal than vertical movement. Varying the dip of the normal faulting source mechanisms by ±20° results in vertical displacement rates of 5%-25% fraction of the horizontal displacement rates. Compared to geologically and geodetically derived displacement rates, which are in the order of 200 μm/a to 500 μm/a vertically and below 500 μm/a horizontally, our estimated coseismic slip only covers less than 10% of the overall deformation. Hence, the URG seems to be dominated by aseismic deformation, even though it coincides with one of the most active seismic zones north of the Alps.

We have shown that the evaluation of earthquake magnitudes as low as M_L 2.0 for *b*-value variations allows a quantitative subdivision of the URG in four sections and provides valuable information for the local determination of earthquake occurrence frequencies that can be adopted for future studies of both seismic hazard assessment and subsurface structural investigations on more local scales.

Acknowledgements

We thank the Erdbebendienst Südwest in Baden-Württemberg and Rheinland-Pfalz in Germany, the French seismic service *RéNaSS*, the Swiss Seismic service *SED* and the *CENEC* project for providing their earthquake bulletins. Special thanks to G. Leydecker and G. Hartmann (BGR) for detailed insights into their bulletins and to J. C. Grimmer and T. Fuhrmann for providing and converting fault data from the southern URG. Many thanks to K.-P. Bonjer and G.H. Eisbacher for discussions and sharing their knowledge on the URG. We also thank Thomas Plenefisch and Benjamin Homuth for their constructive reviews and comments. Figures were made using GMT (Wessel and Smith, 1998).

References

Ahorner, L. & Schneider, G., 1974. Herdmechanismen von Erdbeben im Oberrhein-Graben und in seinen Randgebieten, in *Approaches to Taphrogenesis*, eds Illies, J.H. & Fuchs, K., E. Schweitzerbarth'sche Verlagsbuchhandlung, Stuttgart, 104-117.

Allmann, B., Edwards, B., Bethmann, F. & Deichmann, N., 2010. Determination of MW and calibration of ML (SED) – MW regression (Appendix I), in *ECOS-09 Earthquake Catalogue of Switzerland*, eds Fäh, D. et al., Swiss Seismological Service, ETH Zürich.

Aki, K., 1965. Maximum likelihood estimate of b in the formula log N=a-bM and its confidence limits, *Bull. Earthq. Res. Inst.*, **43**, 237–239.

Barth, A., 2011. Die Erdbeben in Kandel/Südpfalz von 1880 und 1903, *Bautechnik*, **88**, 860-865, doi:10.1002/bate.201101528.

Barth, A., Reinecker, J. & Heidbach, O., 2008. Stress derivation from earthquake focal mechanisms, *World Stress Map Project internal report.* Available at http://dc-app3-14.gfz-potsdam.de/pub/guidelines/-WSM_analysis_guideline_focal_mechanisms.pdf.

Barth, A., Wenzel, F. & Delvaux, D., 2009. Tectonic stress field in rift systems – a comparison of Rhinegraben, Baikal Rift and East African Rift, in *Cahier du Centre Européen de Géodynamique et de Séismologie*, **28**, Proceedings of the Workshop "Seismicity patterns in the Euro-Med region", ed Oth, A., Luxembourg City, 17-19 November 2008, 28, 47-52.

Barth, A., Wenzel, F. & Langenbruch, C., 2013. Probability of earthquake occurrence and magnitude estimation in the post shut-in phase of geothermal projects, *J. Seismol.*, **17**, 5-11, doi:10.1007/s10950-011-9260-9.

Bartz, J., 1974. Die Mächtigkeit des Quartärs im Oberrheingraben, in *Approaches to Taphrogenesis*, eds Illies, J. H. & Fuchs, K Schweizerbarth´sche Verlagsbuchhandlung, Stuttgart, 78-87.

Becker, A. & Paladini, S., 1990. In-situ Spannungen in Nord- und Mitteleuropa, in *Schriftenreihe Angewandte Geologie Karlsruhe*, **10**, eds Czurda, K. & Hötzl, H., Universität Karlsruhe.

Behrmann, J. H., Hermann, O., Horstmann, M., Tanner, D.C. & Bertrand, G., 2003. Anatomy and kinematics of oblique continental rifting revealed: A three-dimensional case study of the southeast Upper Rhine graben (Germany)., *Bull. Am. Assoc. Petrol. Geol.*, 87, 1105-1121.

Bohnhoff, M., Dresen, G., Ellsworth, W.L. & Ito, H., 2010. Passive SeismicMonitoring of Natural and Induced Earthquakes: Case Studies, Future Directions and Socio-Economic Relevance, in *New Frontiers in Inte-*

grated Solid Earth Sciences, International Year of Planet Earth, eds Cloetingh, S., Negendank , J., 261-285, doi 10.1007/978-90-481-2737-5_7.

Bonjer, K.-P., 1997a. Seismicity pattern and style of seismic faulting at the eastern borderfault of the southern Rhine Graben, *Tectonophysics,* **275**, 41-69.

Bonjer, K.-P., 1997b. *nrift.34 catalogue*, Geophys. Inst., Universität Karlsruhe (TH), intern. Report.

Bonjer, K.-P. & Fuchs, K., 1974. Microearthquake-activity observed by a seismic network in the Rhinegraben region, in *Approaches to Taphrogenesis*, eds Illies, J.H. & Fuchs, K., E. Schweitzerbarth'sche Verlags-buchhandlung, Stuttgart, 99-104.

Bonjer, K.-P., Gelbke C., Gilg, B., Rouland, D., Mayer-Rosa, D. & Massinon, B., 1984. Seismicity and dynamics of the Upper Rhinegraben, *J. Geophys.*, **55**, 1-12.

Buness, H., Gabriel, G. & Ellwanger, D., 2008. The Heidelberg Basin drilling Project: Geophysical pre-site surveys, *Quat. Sci. J.*, **57**, 338-366.

Burkhard, M. & Grünthal, G., 2009. Seismic source zone characterization for the seismic hazard assessment project PEGASOS by the Expert Group 2 (EG1b), *Swiss J. Geosci.*, **102**, 149-188.

Cardozo, G. G. O. L. & Behrmann, J. H., 2006. Kinematic analysis of the Upper Rhine Graben boundary fault system, *Journal Of Structural Geology*, *Pergamon-Elsevier Science Ltd*, **28**, 1028-1039.

Cuenot, N., Dorbath, C. & Dorbath, L., 2008. Analysis of the Microseismicity Induced by Fluid Injections at the EGS Site of Soultz-sous-Forêts (Alsace, France): Implications for the Characterization of the Geothermal Reservoir Properties, *Pure Appl. Geophys.*, **165**, 797-828, doi:10.1007/s00024-008-0335-7.

Dahm, T., Becker, D., Bischoff, M., Cesca, S., Dost, B., Fritschen, R., Hainzl, S., Klose, C., Kühn, D., Lasocki, S., Meier, T., Ohrnberger, M., Rivalta, E., Wegler, U. & Husen, S., 2013. Recommendation for the discrimination of human-related and natural seismicity, *J. Seismol.*, **17**, 197-202, doi:10.1007/s10950-012-9295-6.

Deichmann, N., 2009. Conversion of local magnitude from foreign catalogs to SED local magnitude (Appendix K), in *ECOS-09 Earthquake Catalogue of Switzerland*, eds Fäh, D. et al., Swiss Seismological Service, ETH Zürich.

Deichmann, N. & Giardini, D., 2009. Earthquakes induced by the stimulation of an enhanced geothermal system below Basel (Switzerland), *Seismol. Res. Lett.*, **80**, 784–798.

Delacou, B., Sue, C., Champagnac, J.-D. & Burkhard, M., 2004. Present-day geodynamics in the bend of the western and central Alps as constrained by earthquake analysis, *Geophys. J. Int.*, **158**, 753-774.

DIN 4149 (2005). *DIN4149:2005-04 Bauten in deutschen Erdbebengebieten - Lastannahmen, Bemessung* *und Ausführung üblicher Hochbauten*, Deutsches Institut für Normung e.V., Berlin.

Edel, J.-B., Whitechurch, H. & Diraison, M., 2006. Seismicity wedge beneath the Upper Rhine Graben due to backwards Alpine push?, *Tectonophysics*, **428**, 49-64.

Evans, K. F., Zappone, A., Kraft, T., Deichmann, N. & Moia, F., 2012. A survey of the induced seismic responses to fluid injection in geothermal and CO2 reservoirs in Europe, *Geothermics,* **41**, 30-54.

Fäh, D., Giardini, D., Kästli, P., Deichmann, N., Gisler, M., Schwarz-Zanetti, G., Alvarez-Rubio, S., Sellami, S., Edwards, B., Allmann, B., Bethmann, F., Wössner, J., Gassner-Stamm, G., Fritsche, S., Eberhard, D., 2011. *ECOS-09 Earthquake Catalogue of Switzerland, Release 2011, Report and Database*, Report SED/RISK/R/001/20110417, Swiss Seismological Service ETH Zurich.

Fäh, D., Gisler, M., Jaggi, B., Kästli, P., Lutz, T., Masciadri, V., Matt, C., Mayer-Rosa, D., Rippmann, D., Schwarz-Zanetti, G., Tauber, J. & Wenk, T., 2009. The 1356 Basel earthquake: an interdisciplinary revision, *Geophys. J. Int.*, **178**, 351-374, doi:10.1111/j.1365-246X.2009.04130.x.

Fielitz, W., Eisbacher, G. H. & Grimmer, J., 2014. Late-Variscan W-dipping lithospheric detachment and granite emplacement in the basement of the Upper Rhine Graben shoulder, *Schr.reihe Dtsch. Ges. Geowiss.*, **85**, 604.

Fuhrmann, T., Heck, B., Knöpfler, A., Masson, F., Mayer, M., Ulrich, P., Westerhaus, M. & Zippelt, K., 2013. Recent surface displacements in the Upper Rhine Graben - Preliminary results from geodetic networks, *Tectonophysics*, **602**, 300-315.

Fuhrmann, T., Westerhaus, M., Zippelt, K. & Heck, B., 2014. Vertical displacement rates in the Upper Rhine Graben area derived from precise leveling, *J. Geod.*, doi:10.1007/s00190-014-0721-0.

Gaßner, L., Groos, J. & Ritter, J.R.R., 2014. Herdflächenanalyse induzierter Erdbeben in der Südpfalz: Reaktivierung präexistenter Bruchflächen und Spannungszustand. *Mainzer Geowissenschaftliche Mitteilungen*, in press.

GeORG-Team, 2013. *Geopotenziale des tiefen Untergrundes im Oberrheingraben*, Fachlich-technischer Abschlussbericht des Interreg-Projekts GeORG. Available at http://www.geopotenziale.org.

Greiner, G. & Illies, J.H., 1977. Central Europe: active or residual tectonic stresses. Pure Appl. Geophys., **115**, 11-26.

Grellet, B., Combes, P., Granier, T. & Philip, H., 1993. Sismotectonique de la France métropolitaine 1 & 2, *Mém. Soc. Géol. Fr.*, **164**, 76p/24p.

Grünthal, G. & Bosse, C., 1996. *Probabilistische Karte der Erdbebengefährdung der Bundesrepublik Deutschland - Erdbebenzonierungskarte für das Nationale Anwendungsdokument zum Eurocode 8*, Geoforschungszentrum Potsdam (GFZ), Forschungsbericht.

Grünthal, G., Bosse, C., Sellami, S., Mayer-Rosa, D. & Giardini, D., 1999. Compilation of the GSHAP regional seismic hazard for Europe, Africa and the Middle East, *Ann. Geofis.,* **42**, 1215-1223.

Grünthal, G., Mayer-Rosa, D. & Lenhardt, W. A., 1998. Abschätzung der Erdbebengefährdung für die D-A-CH- Staaten – Deutschland, Österreich, Schweiz, *Bautechnik,* **75**, 753-767.

Grünthal, G., Stromeyer, D. & Wahlström, R., 2009. Harmonization check of Mw within the central, northern, and northwestern European earthquake catalogue (CENEC), *J. Seismol.*, **13**, 613-632.

Grünthal, G. & Wahlström, R., 2003. An Mw based earthquake Catalogue for central, northern and northwestern Europe using a hierarchy of magnitude conversions, *J. Seismol.*, **7**, 507-531, doi:10.1023/B:JOSE.0000005715.87363.13.

Helm, J.A., 1996. The natural seismic hazard and induced seismicity of the European HDR (Hot Dry Rock) geothermal energy project at Soultz-sous-Forêts, France, *Ph.D. thesis*, Univ. Louis-Pasteur, Strasbourg, France.

Hiemer, S., Woessner, J., Basili, R., Danciu, L., Giardini, D. & Wiemer, S., 2014. A smoothed stochastic earthquake rate model considering seismicity and fault moment release for Europe, *Geophys. J. Int.*, **198**, 1159-1172.

Hiller, W., Rothe, J.-P. & Schneider, G., 1967. La seismicite du fosse rhenan, in *The Rhinegraben Progress Report 1967*, eds Rothe, J.-P. & Sauer, K., *Ahb. Geol. Landesamt Baden-Württemberg*, **6**, 98-100 & 2 figures.

Homuth, B., Rümpker, G., Deckert, H. & Kracht, M., 2014. Seismicity of the northern Upper Rhine Graben - Constraints on the present-day stress field from focal mechanisms, *Tectonophysics*, **632**, 8-20, doi:10.1016/j.tecto.2014.05.037.

Jackson, J. & McKenzie, D., 1988. The relationship between plate motions and seismic moment tensors, and the rates of active deformation in the Mediterranean and Middle-East, *Geophys. J. Roy. Astr. Soc.*, **93**, 45-73.

Kostrov, V. V., 1974. Seismic moment and energy of earthquakes, and seismic flow of rocks, *Izv. Acad. Sci. USSR Phys. Solid Earth*, **1**, 23-44.

Kreemer, C., Klein, G.E., Shen, Z.-K., Wang, M., Estey, L., Wier, & Boler, F., 2014. *Global geodetic strain rate model. GEM Technical Report 2014*, 07 V1.0.0, 129 pp., GEM Foundation, Pavia, Italy, doi: 10.13117/GEM.GEGD.TR2014.07.

Leydecker, G., 2011. Erdbebenkatalog für Deutschland mit Randgebieten für die Jahre 800 bis 2008. *Geo-*

log. Jahrb., **E59**, Schweitzerbart'sche Verlagsbuchhandlung, Stuttgart.

Lippert, W., 1979. *Erstellung von Formeln für die Magnitudenbestimmung von Nahbeben sowie Seismizität der Jahre 1971-1978 im Bereich des Oberrheingrabens*. Diplomarbeit (unpublished), Geophysical Institute, Universität Karlsruhe (TH).

Mayer, G., Mai, P.M., Plenefisch, T., Echtler, H., Lüschen, E., Wehrle, V., Müller, B., Bonjer, K.-P., Prodehl, C., Fuchs, K., 1997. The deep crust of the Southern Rhine Graben: reflectivity and seismicity as images of dynamic processes. *Tectonophysics*, **275**, 15-40.

Meier, L. Eisbacher, G.H., 1991. Crustal kinematics and deep structure of the northern Rhine graben, Germany, *Tectonics*, **10**, 621-630.

Mignan, A. & Wössner J., 2012. Estimating the magnitude of completeness for earthquake catalogs, *Community Online Resource for Statistical Seismicity Analysis*, doi:10.5078/corssa-00180805. Available at *http://www.corssa.org*.

Müller, B., Wehrle, V., Zeyen, H. & Fuchs, K., 1997. Short-scale variations of tectonic regimes in the western European stress province north of the Alps and Pyrenees, *Tectonophysics*, **275**, 199-219.

Nivière, B., Brüstle, A., Bertrand, G., Carretier, S., Behrmann, J. & Gourry, J.-C., 2008. Active tectonics of the southeastern Upper Rhine Graben, Freiburg area (Germany), *Quat. Sci. Rev.*, **27**, 541-555.

Page, R., 1968. Aftershocks and microaftershocks of the great Alaska earthquake of 1964, *Bull. Seism. Soc. Am.*, **58**, 1131-1168.

Peters, G., 2007. Active Tectonics in the Upper Rhine Graben - Integration of paleoseismology, geomorphology and geomechanical modeling, *Ph.D thesis*, Vrije Universiteit Amsterdam, Netherlands.

Plenefisch, T. & Bonjer, K. P., 1997. The stress field in the Rhine Graben area inferred from earthquake focal mechanisms and estimation of frictional parameters, *Tectonophysics*, *Stress and Stress Release in the Lithosphere - Structure and Dynamic Processes in the Rifts of Western Europe*, **275**, 71-97.

Prinz, H. & Schwarz, E., 1970. Nivellement und rezente tektonische Bewegungen im nördlchen Oberrheingraben, in *Graben Problems*, eds Illies, J. H. & Mueller, St., Schweizerbarth´sche Verlagsbuchhandlung, Stuttgart, 177-183.

Prodehl, C., Ansorge, J., Edel, J.B., Emter, D., Fuchs, K., Mueller, S., Peterschmitt, E., 1976. Explosion-seismlogy research in the Central and Southern Rhine Graben – a case history, in *Explosion Seismology in Central Europe*, eds Giese, P., Prodehl, C. & Stein, A., Springer-Verlag, Berlin, 313-328.

Reinecker, J., Tingay, M., Müller, B. & Heidbach, O., 2010. Present-day stress orientation in the Molasse Basin, *Tectonophysics*, 482, 129-138.

Ritter, J. R. R. & Groos, J., 2014. Abschlussbericht MAGS-EP1, Quantifizierung und Charakterisierung des induzierten seismischen Volumens im Bereich Landau/Südpfalz. Available at http://www.mags--projekt.de/MAGS/DE/Downloads/MAGS_Abschlussbericht_EP1.pdf

Ritter, J. R. R., Wagner, M., Bonjer, K.-P. & Schmidt, B., 2009. The 2005 Heidelberg and Speyer earthquakes and their relationship to active tectonics in the central Upper Rhine Graben, *Int. J. Earth Sci. (Geol. Rundsch.),* **98**, 697-705.

Rotstein, Y., & M. Schaming, 2008. Tectonic implications of faulting styles along a rift margin: The boundary between the Rhine Graben and the Vosges Mountains, *Tectonics*, **27**, doi:10.1029/2007TC002149.

Rotstein, Y., Schaming, M. & Rousse, S., 2005a. Structure and Tertiary tectonic history of the Mulhouse High, Upper Rhine Graben: Block faulting modified by changes in the Alpine stress regime,Tectonics, **24**, TC1012, doi:10.1029/2004TC001654.

Rotstein, Y., Schaming, M. & Rousse, S., 2005b. Tertiary tectonics of the Dannemarie Basin, upper Rhine graben, and regional implications, *Int. J. Earth Sci.*, **94**, 669-679, doi:10.1007/s00531-005-0473-4.

Rózsa, S., Mayer, M., Westerhaus, M., Seitz, K. & Heck, B., 2005. Towards the determination of displacements in the Upper Rhine Graben area using GPS measurements and precise antenna modelling, *Quat. Sci. Rev.*, **24**, 425-438.

Schmedes, J., Hainzl, S., Reamer, S.-K., Scherbaum, F. & Hinzen, K.-G., 2005. Moment release in the Lower Rhine Embayment, Germany: seismological perspective of the deformation process, *Geophys. J. Int.*, **160**, 901-909.

Schumacher, M. E., 2002. Upper Rhine Graben: Role of preexisting structures during rift evolution, *Tectonics*, **21**, 1006, doi:10.1029/2001TC900022.

Schweizerischer Erdbebendienst (SED), 2002. ECOS – Earthquake Catalogue of Switzerland. *Report to PEGASOS, Version 31.03.2002*, ETH Zürich, 95.p.

Stange, S., 2006. ML Determination for Local and Regional Events Using a Sparse Network in Southwestern Germany, *J. Seismol.*, **10**, 247-257.

Tesauro, M., Hollenstein, C., Egli, R., Geiger, A. & Kahle, H.-G., 2006. Analysis of central western Europe deformation using GPS and seismic data, J. Geodyn., **42**, 194-209.

Utsu, T., 1965. A method for determining the value of b in a formula log n=a-bM showing the magnitude-frequency relations for earthquakes, *Geophys. Bull. Hokkaido Univ.,* **13**, 99-103.

Weichert, D. H., 1980. Estimation of the earthquake recurrence parameters for unequal observation periods for different magnitudes, *Bull. Seism. Soc. Am.*, 70, 1337-1346.

Wenzel, F. & Brun, J.-P., 1991. A deep reflection seismic line across the Northern Rhine Graben, *Earth Planet. Sci. Lett.*, **104**, 140-150.

Wessel, P. & Smith, W. H. F., 1998. New, improved version of Generic Mapping Tools released, *EOS, Trans. AGU*, **79**, 579pp.

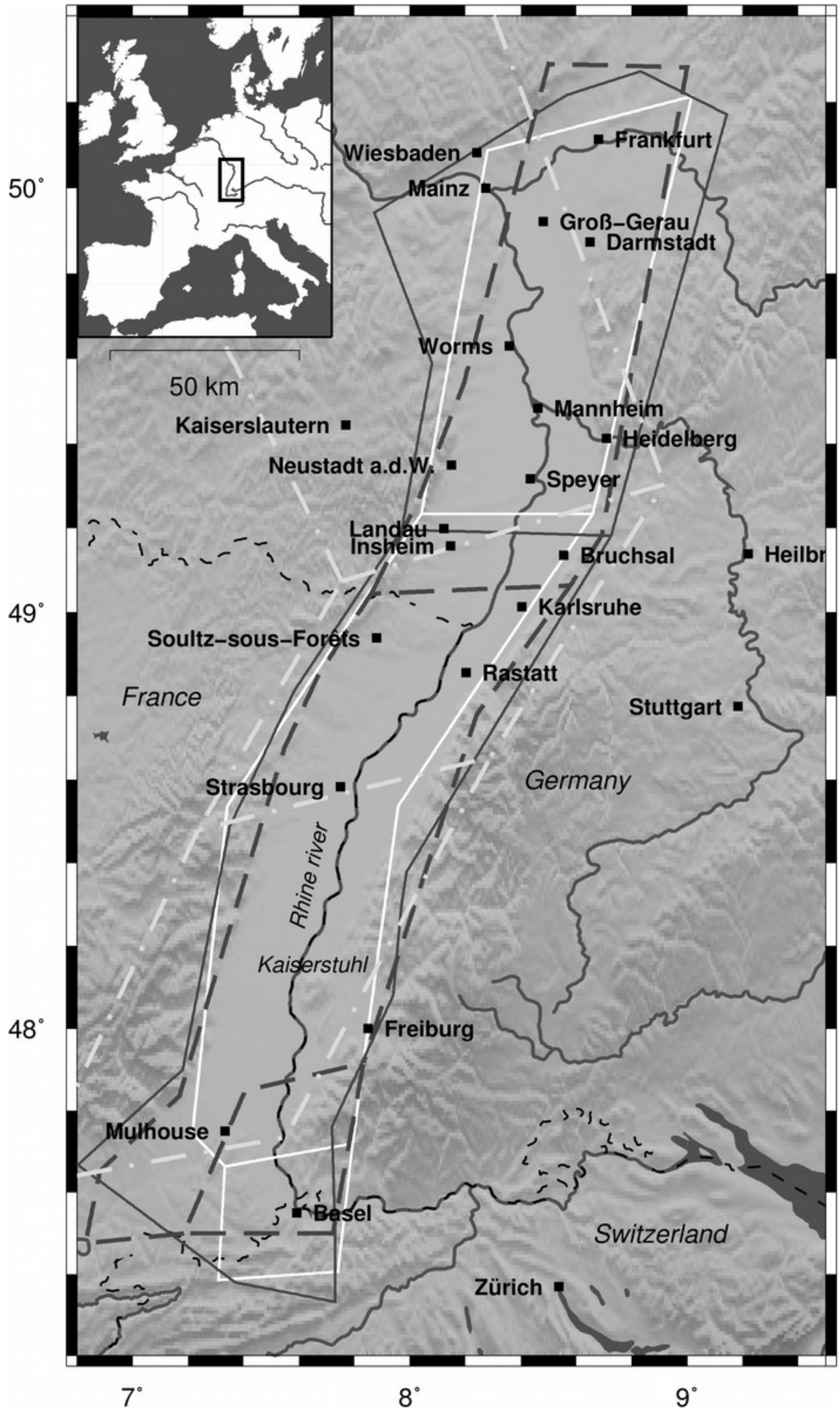

Figure 1: Seismo-tectonic zones in the Upper Rhine Graben after Leydecker (2011, grey solid line), GSHAP (Grünthal et al., 2009 , white solid), Helm (1996, white dash-dotted), and Burkhard & Grünthal (2009; dashed grey).

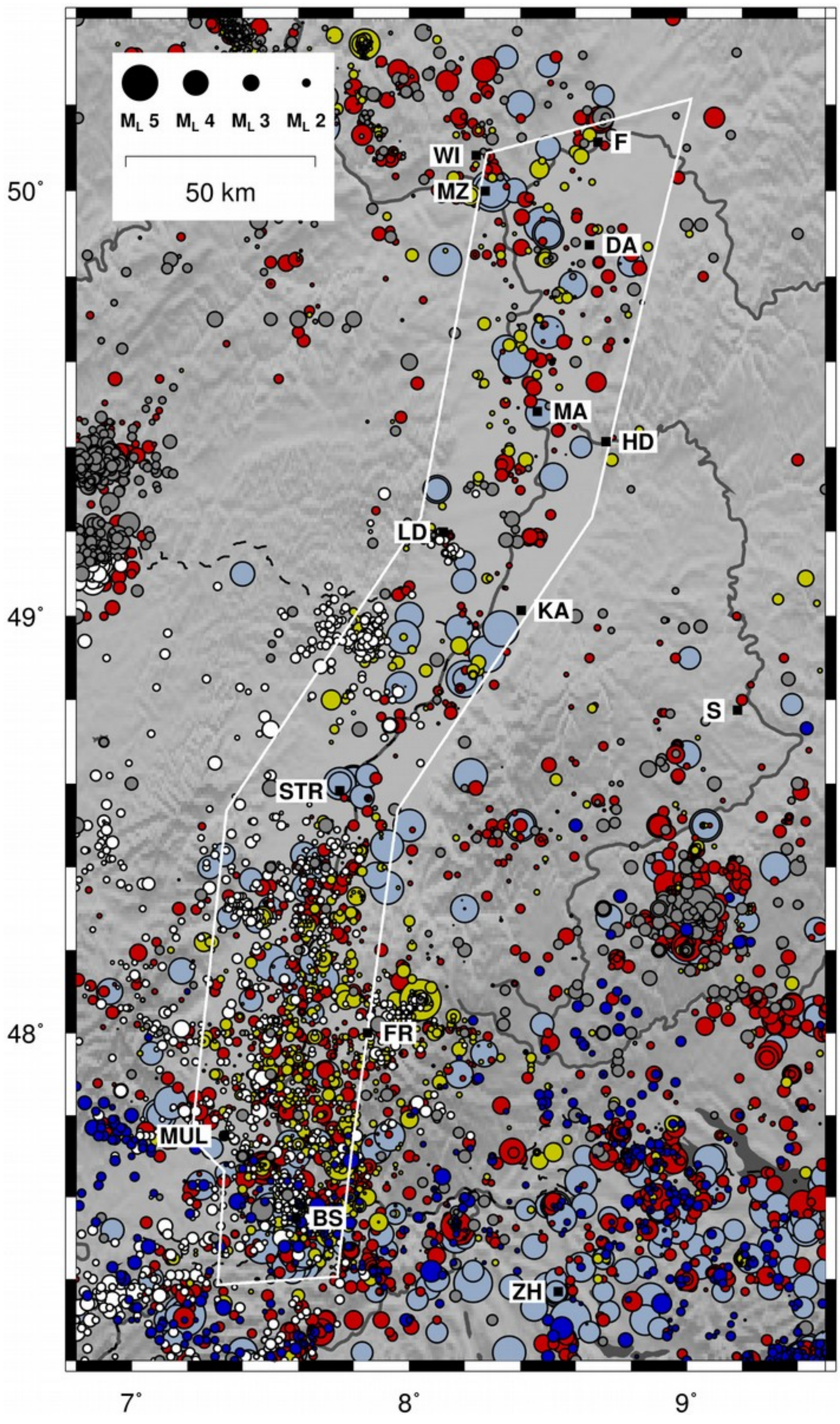

Figure 2: Seismicity of the Upper Rhine Graben 1250-02/2012 taken from the catalogues of *LGRB* (yellow), *nrift* (red), *RéNaSS* (white), *BGR* (black), *ECOS* (dark blue), and *CENEC* (light blue). Size of circles scales with local *LGRB*-Magnitude M_L. The white frame marks the seismo-tectonic zones after Grünthal et al. (2009).

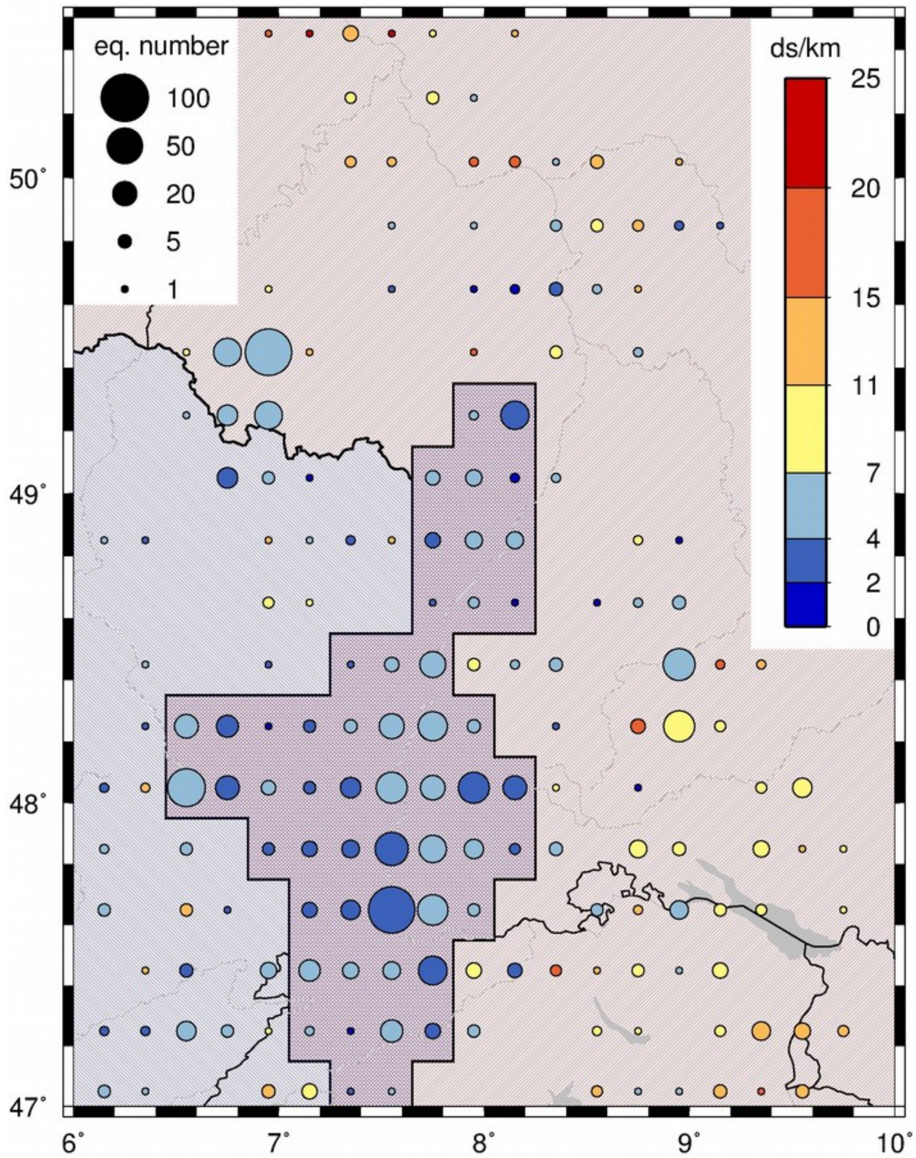

Figure 3: Double listed events contained in both the *LGRB*/*nrift* and the *RéNaSS*/*LDG* catalogues between 1980 and 2012. Circles show average location difference ds (colour scale) and number of corresponding events (size of circles) within each grid cell. The hatched areas mark the regions for reliable localisation by the *LGRB* (red) and the *RéNaSS* (blue) catalogue. The double hatched area indicate the area of reliable locations from both agencies along the URG.

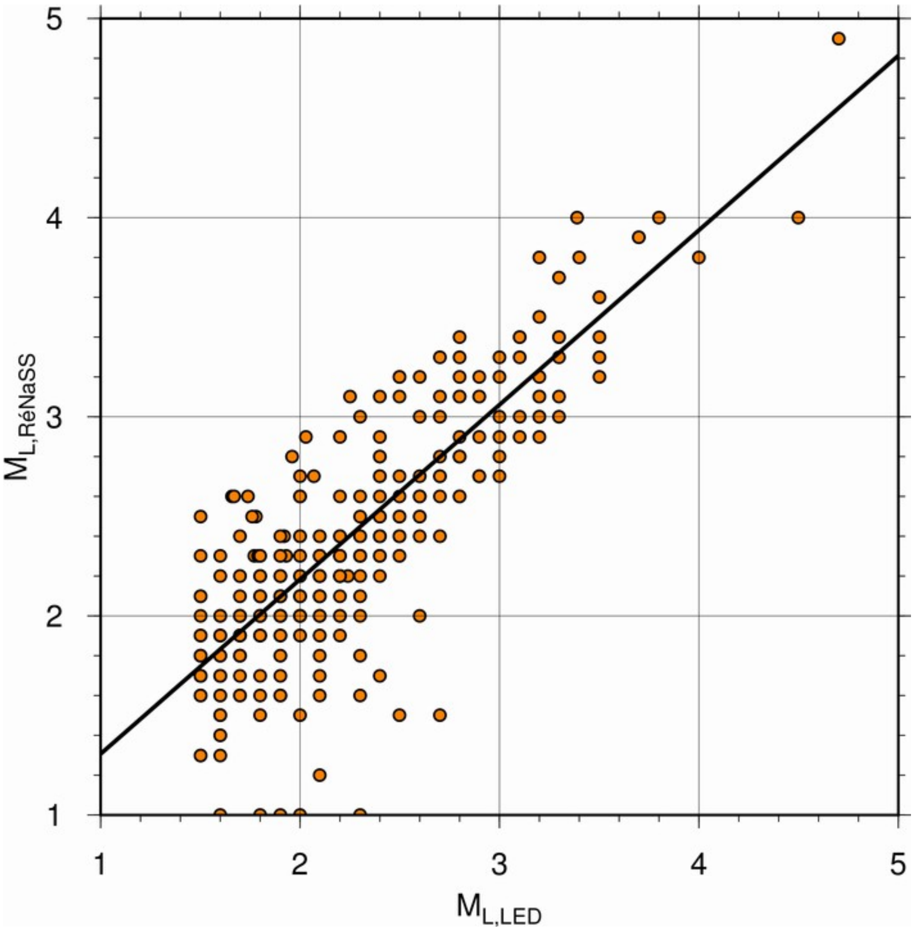

Figure 4: Linear regression between local magnitudes M_L in the URG of double listed earthquakes contained in both the *LED*/*nrift* and *RéNaSS*/*LDG* catalogue between 1980 and 2012. Only events within the area of reliable localisations of both agencies are used (see Fig. 3).

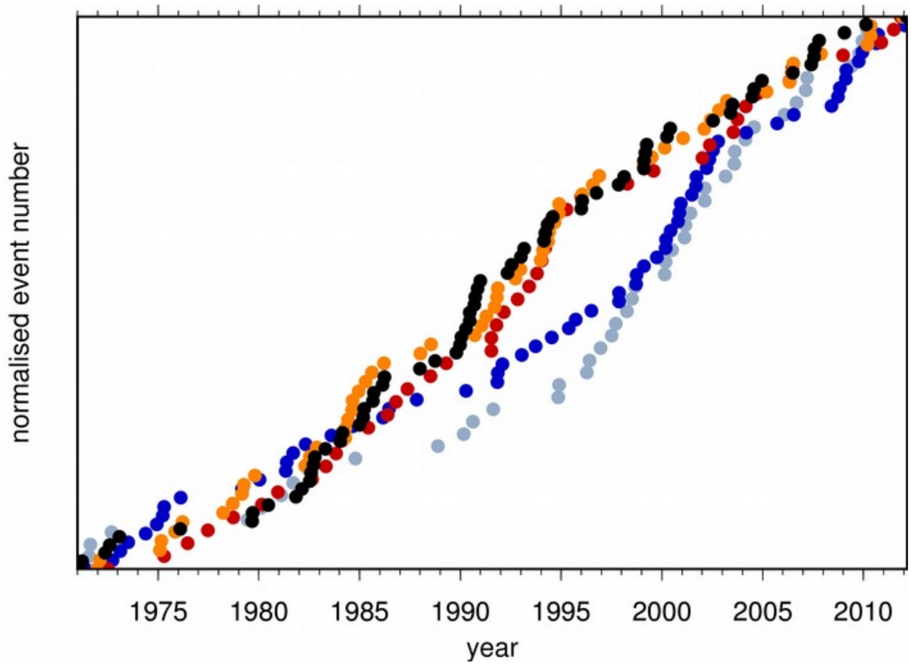

Figure 5: Cumulative numbers of earthquakes since 1971 for 0.1 wide magnitude ranges around M_L 1.8 (light blue), M_L 1.9 (dark blue), M_L 2.0 (black), M_L 2.1 (orange), and M_L 2.2 (red). For each magnitude range numbers are scaled to maximum.

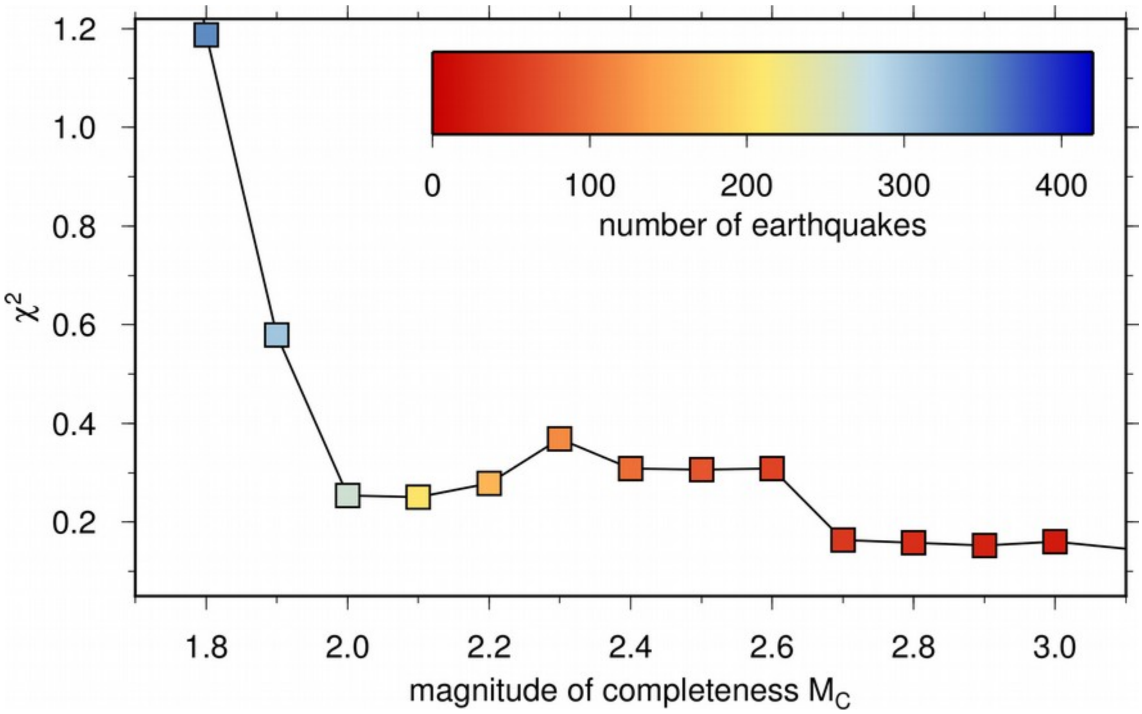

Figure 6: Chi-squared test for different magnitudes of completeness M_C for earthquakes since 1982 in the URG. The number of events with $M_L \geq M_C$ is coloured by the number of earthquakes available.

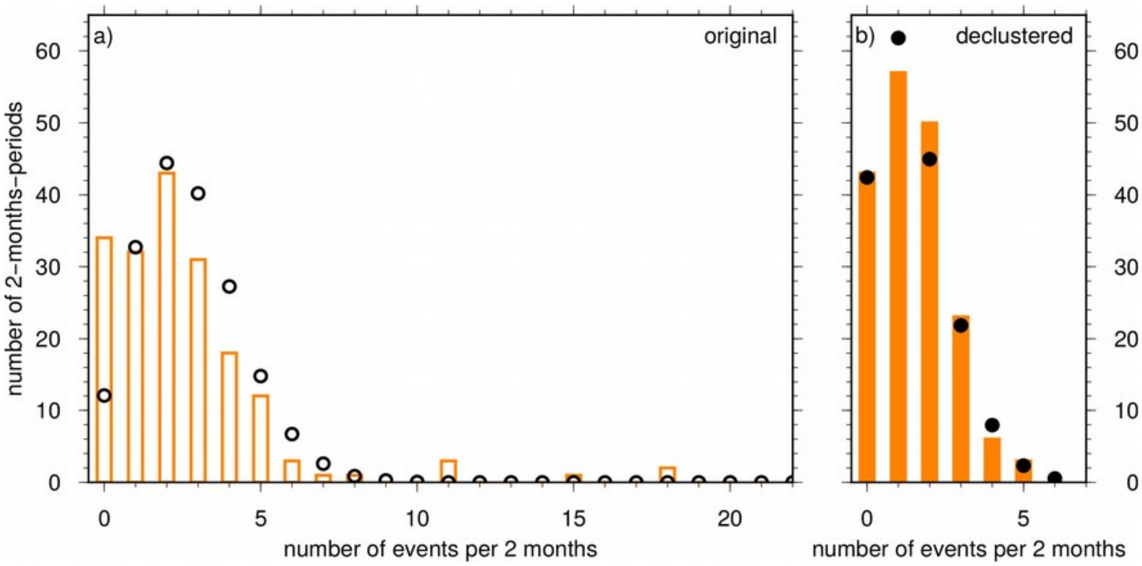

Figure 7: Number of seismic events above the magnitude of completeness of $M_L \geq 2.0$ since 1982 during periods of two months (orange bars) : (a) original dataset and (b) declustered dataset. Dots indicate a perfect Poisson distribution.

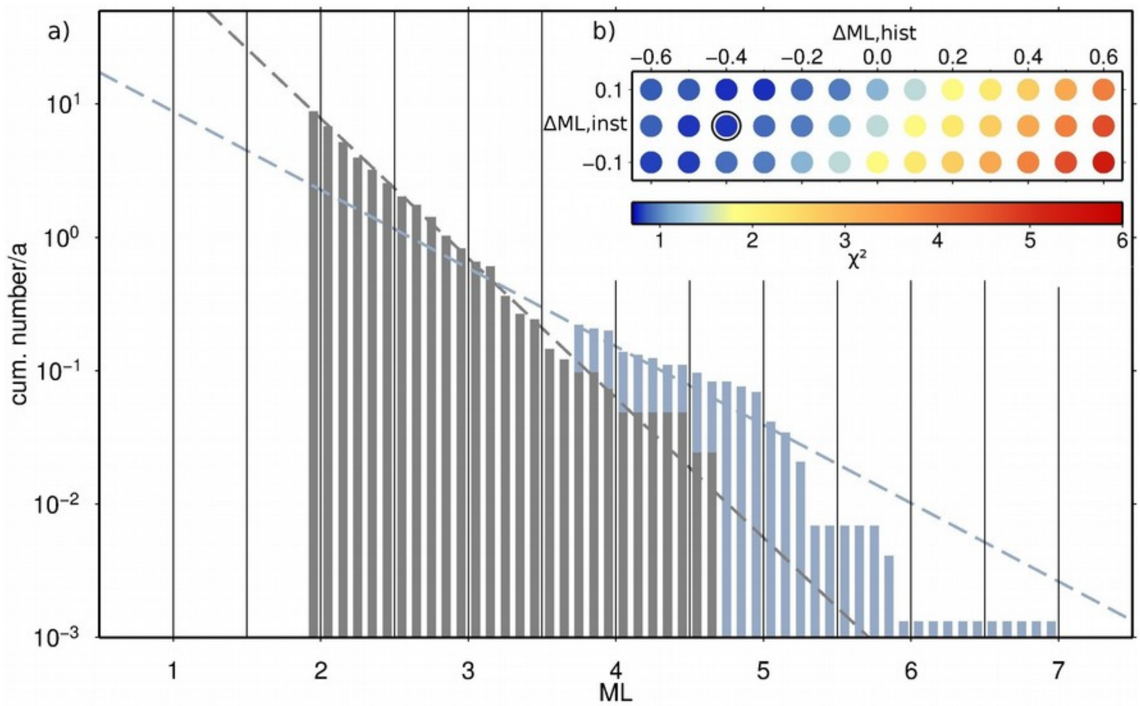

Figure 8: (a) Cumulative magnitude-frequency distribution of instrumental (grey) and historic (light blue) earthquakes with maximum likelihood fit for the whole URG. (b) Chi-squared test for shifting historic magnitudes $\Delta M_{L,hist}$ against instrumentally determined $\Delta M_{L,inst}$. The black circle marks the best fitting shift.

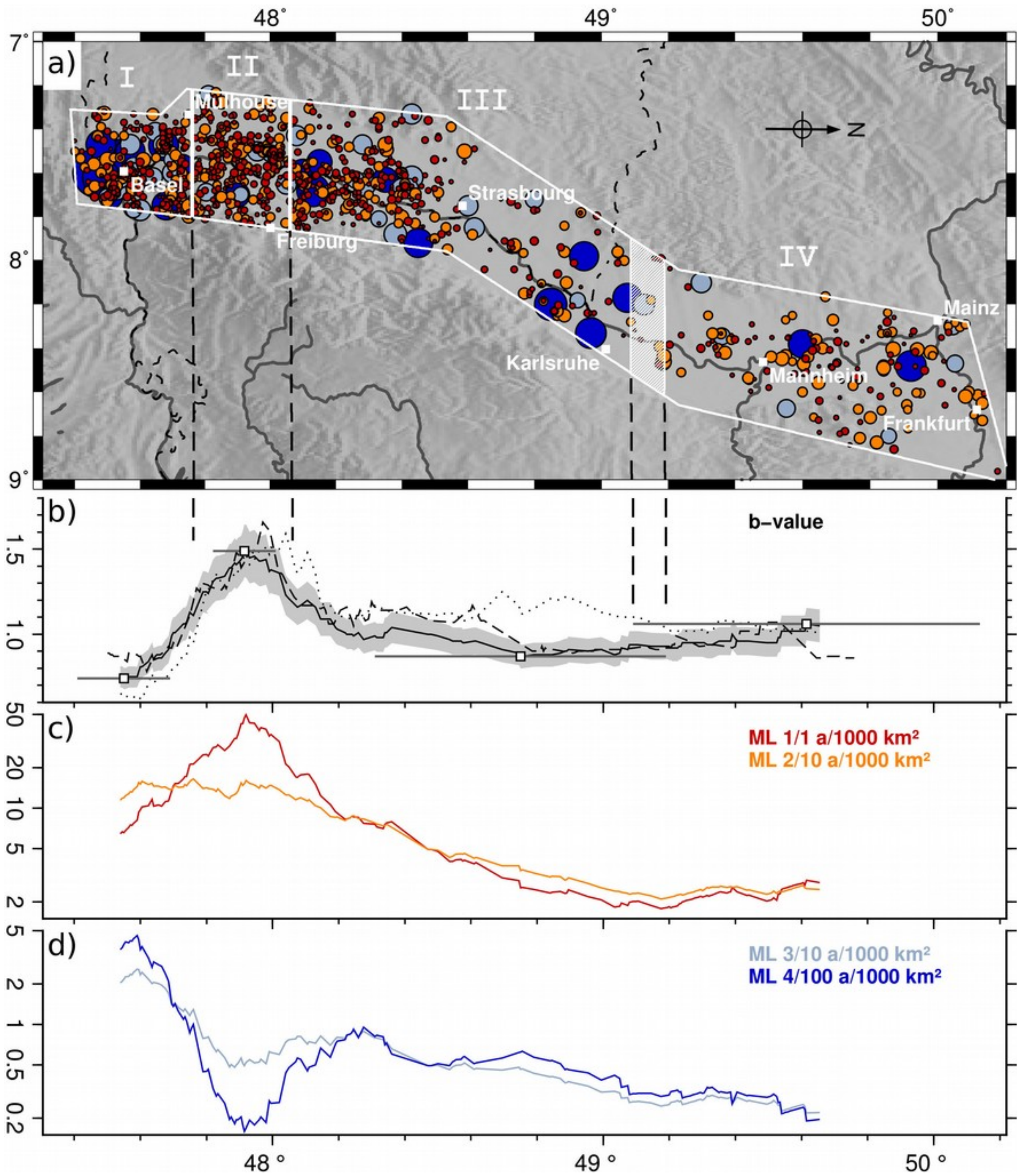

Figure 9: Result of the regional magnitude-frequency analysis for the URG. (a) Declustered earthquake dataset $M_L \geq 1.0$ (colourisation according to subfigures c) and d) and new subdivision of the URG in sections I to IV (see text). (b) Solid line: *b*-values for overlapping regions (each containing 50 events $M_L \geq 2.0$). The shaded area gives the standard deviations. Dotted line: without historic earthquakes; dashed line: dataset without declustering. White squares show *b*-value extrema, the grey horizontal lines indicate the lateral extend of the spatial windows. (c)+(d) Average event rates normalised to an area of 1000 km² for $M_L \geq 1.0$ and $M_L \geq 2.0$ (c) as well as $M_L \geq 3.0$ an $M_L \geq 4.0$ (d).

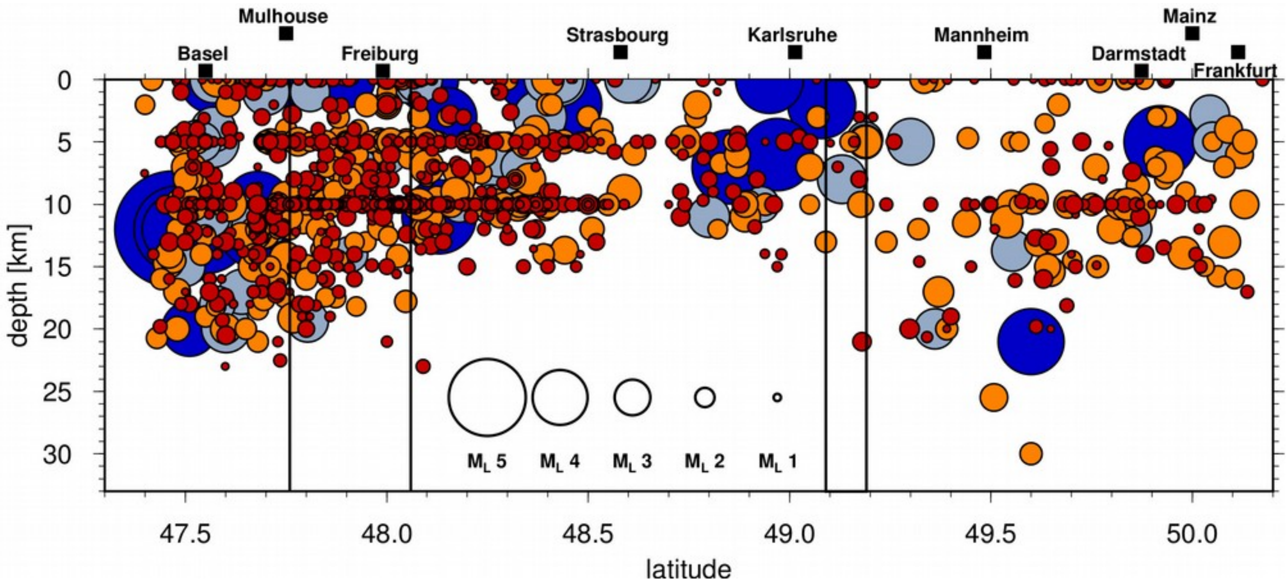

Figure 10: Depth distribution of the declustered earthquake dataset $M_L \geq 1.0$ (colourisation and URG sections according to Fig. 9) and new subdivision of the URG (see text).

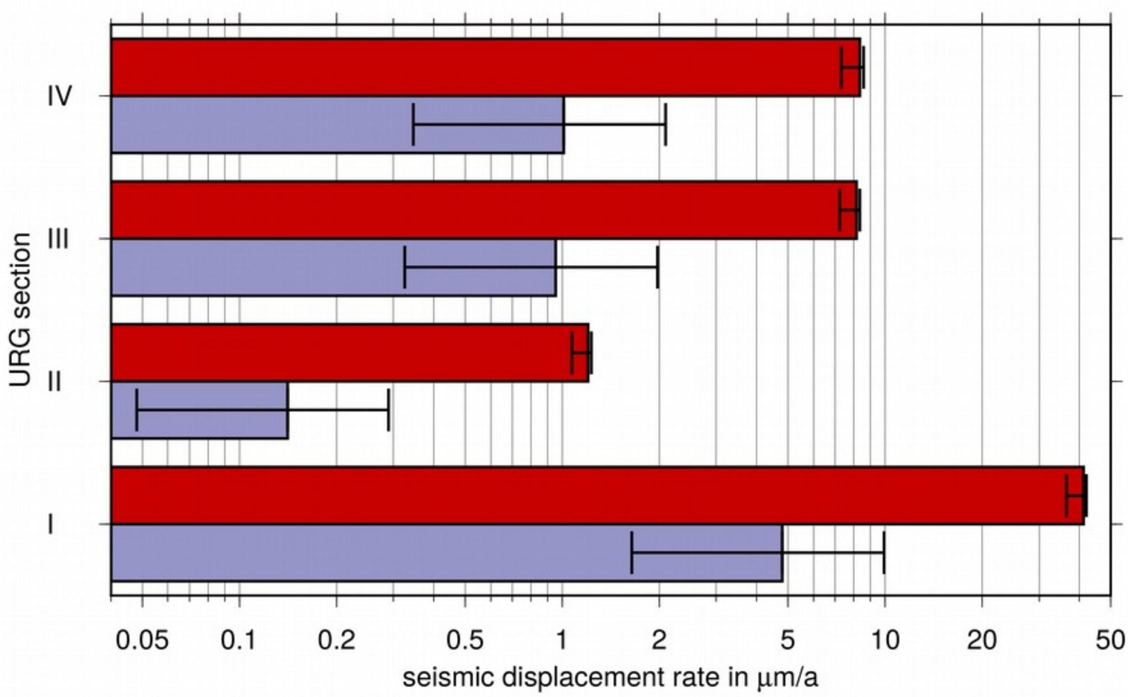

Figure 11: Horizontal (red) and vertical (blue) seismic displacement rates for each section of the URG. The rates were calculated from representative focal mechanisms and cumulative seismic moment rates based on GR magnitude-frequency distributions for the upper crust including fore- and aftershocks (see text). Coloured bars show results for normal faulting mechanisms dipping 60°. Error bars show the variation of the rates when steep (80°) and shallow dipping (40°) fault planes are used.

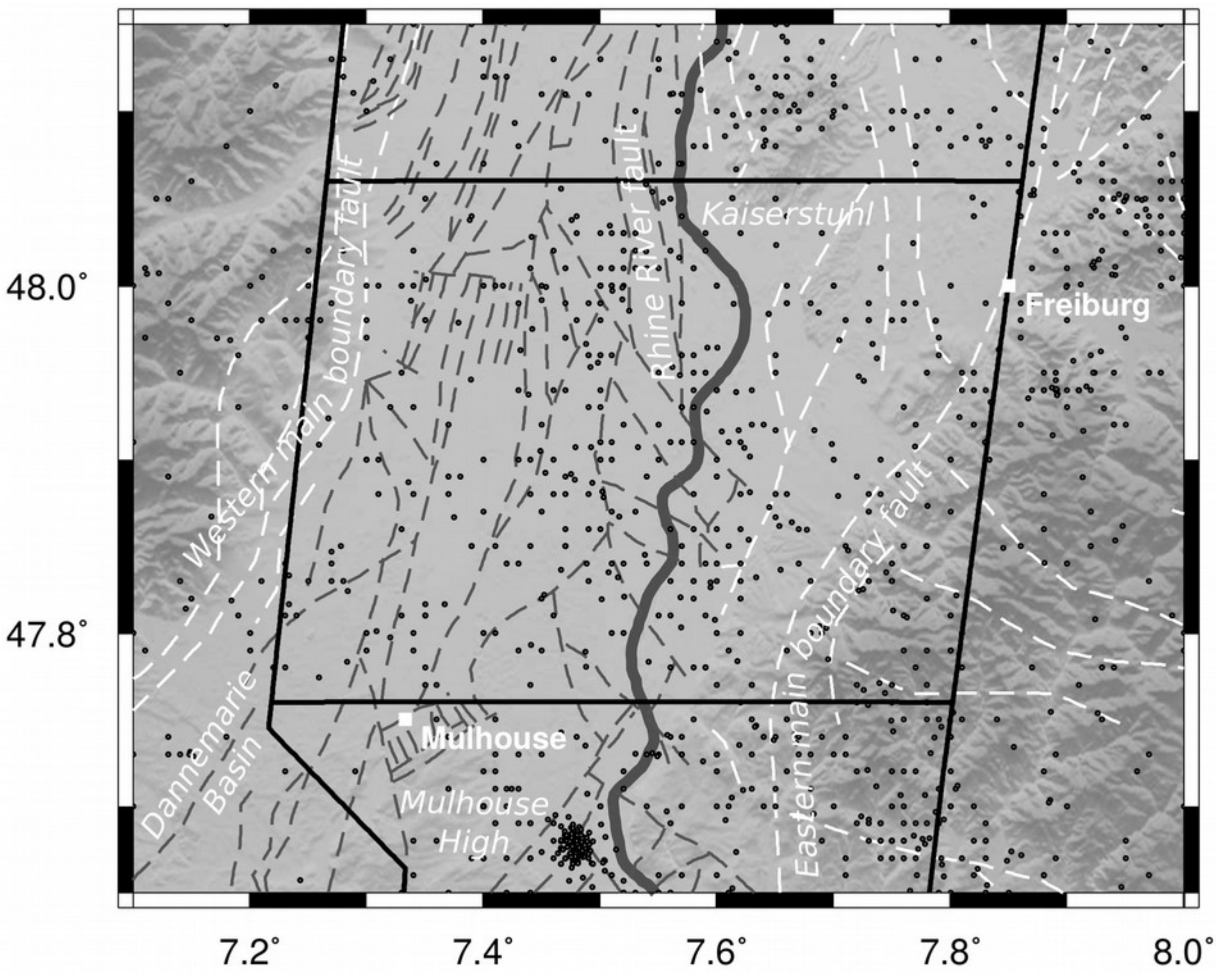

Figure 12: Fault structure and seismicity in the URG section II (black frame). Grey dashed lines: faults at the top of the crystallin redrawn after GeORG-Team (2013). White dashed lines: faults at the graben boundaries redrawn after Peters (2007). Dots show earthquakes of $M_L \geq 0.0$. The cluster SE of Mulhouse corresponds to earthquake series near Sierentz/France in the 1980's.